Electronic Supplementary Information

In situ construction of phenanthroline-based cationic radical porous hybrid polymers for metal-free heterogeneous catalysis

Guojian Chen,* Yadong Zhang, Ke Liu, Xiaoqing Liu, Lei Wu, Hu Zhong, Xuejing Dang, Minman Tong and Zhouyang Long*

School of Chemistry and Materials Science, Jiangsu Key Laboratory of Green Synthetic Chemistry for Functional Materials, Jiangsu Normal University, Xuzhou, 221116, China.

*E-mail: gjchen@jsnu.edu.cn (G. Chen); longzhouyangfat@163.com (Z. Long)

Materials

Raw materials including octavinylsilsesquioxane (HWRK), 3,8-dibromo-1,10-phenanthroline (Yanshen Technology), 1,10-phenanthroline, 1,10-phenanthroline hydrate, tetrakis(triphenylphosphine)-palladium(0), K_2CO_3, 1,2-dibromoethane, bromoethane, and other reactants and solvents are commercially available and used without further purification.

Methods

Liquid-state ^{1}H and ^{13}C NMR spectra of ionic monomers and products were measured with a Bruker DPX 500 spectrometer. Solid-state ^{13}C cross-polarization/magic angle spinning (CP/MAS) and ^{29}Si MAS NMR spectra were recorded on a Bruker AVANCE III 600 spectrometer. Fourier transform infrared spectroscopy (FTIR) was recorded on a Bruker Vertex 80V FT-IR instrument (KBr discs) in the region 4000-400 cm^{-1}. Solid UV-visible adsorption spectra were measured with a SHIMADZU UV-2600 spectrometer. Chemical compositions and states of the materials were determined by the X-ray photoelectron spectroscopy (XPS, Thermo ESCALAB 250Xi). The residual metal Pd was determined by inductively coupled plasma-mass spectrometry (ICP-MS). Electron paramagnetic resonance (EPR) spectra were recorded on a Bruker EMX-10/12 spectrometer using the X-band at room temperature. The CHN elemental analysis was performed on an elemental analyzer Vario EL cube. Thermogravimetric analysis (TGA) was carried out with a TA Q50 instrument under air atmosphere at a heating rate of 10 $^{o}C\ min^{-1}$. X-ray diffraction (XRD) patterns were collected on the Bruker D8 Advance powder diffractometer using Ni-filtered Cu Ka radiation source at 40 kV and 20 mA, from 5 to 80^{o} with a scan rate of 0.2^{o} s^{-1}. Field emission scanning electron microscope (FESEM, Hitachi SU8010) accompanied by Energy dispersive X-ray spectrometry (EDS) was used to study the morphology and the elemental distribution. Transmission electron microscopy (TEM) images were performed on the JEOL JEM-2100F 200 kV field-emission transmission electron microscopes. N_2 adsorption-desorption isotherms were measured at 77 K using a Quantachrome autosorb iQ2 analyzer, and surface areas of samples were calculated by the Brunauer-Emmett-Teller (BET) method and pore size distributions were determined by the nonlocalized density functional theory (NLDFT) model. All the samples were degassed at 150°C for 10 h in high vacuum before analysis.

Synthesis of phenanthroline-based ionic monomers

The phenanthroline ionic monomers were prepared by the one-step quaternization reaction, as shown in Scheme S1. Typically, 3,8-dibromo-1,10-phenanthroline (DBPhen, 5 mmol, 1.69 g) was dispersed in 1,2-dibromoethane (DCE,

25 mL) that was used as both solvent and reactant in the reaction. Then, the mixed suspension solution was treated within a Teflon-lined autoclave in a drying oven at 100°C for 48 h. After reaction, the formed orange-yellow solid was dispersed into THF (40 mL) with vigorous stirring for 2 h. At last, the above suspension was filtrated, washed with THF for several times, and dried at 80°C for 12 h in vacuum to give an orange-yellow crystalline solid [DBPhenEt]Br_2 (denoted as iDBPhen) with a desired yield of 85%. Besides, the dibromo-free phenanthroline dicationic monomer [PhenEt]Br_2 (iPhen-1), a yellow powder solid with a high yield of 91%, was similarly prepared by the reaction of 1,10-phenanthroline with DCE. The control phenanthroline monocationic monomer [PhenEt]Br (iPhen-2), a yellow powder solid with a high yield of 90%, was also prepared by the reaction of 1,10-phenanthroline with excess bromoethane.

N,N'-ethyl-3,8-dibromo-1,10-phenanthrolinium dibromide [DBPhenEt]Br_2: ^{1}H NMR (300 MHz, D_2O) (Fig. S1A): δ (ppm)=9.90 (CH, 2H), 9.69 (CH, 2H), 8.55 (CH, 2H), 5.61 (CH_2, 4H). ^{13}C NMR (75.5 MHz, D_2O) (Fig. S1B): δ (ppm)=150.39, 149.32, 131.86, 130.07, 127.71, 122.17, 52.39. Elemental analysis: Found: C, 32.04; H, 1.79; N, 5.43 wt%. Calcd. for $C_{14}H_{10}N_2Br_4$: C, 31.98; H, 1.92; N, 5.33 wt%.

N,N'-ethyl-1,10-phenanthrolinium dibromide [PhenEt]Br_2: ^{1}H NMR (300 MHz, D_2O) (Fig. S2A): δ (ppm)=9.58~9.56 (CH, 2H), 9.47~9.45 (CH, 2H), 8.63 (CH, 2H), 8.56~8.53 (CH, 2H), 5.64 (CH_2, 4H). ^{13}C NMR (75.5 MHz, D_2O) (Fig. S2B): δ (ppm)=148.61, 148.19, 131.87, 129.89, 128.96, 127.57, 52.29. Elemental analysis: Found: C, 45.62; H, 3.34; N, 7.45 wt%. Calcd. for $C_{14}H_{12}N_2Br_2$: C, 45.68; H, 3.29; N, 7.61 wt%.

N-ethyl-1,10-phenanthrolinium bromide [PhenEt]Br: ^{1}H NMR (300 MHz, D_2O) (Fig. S3A): δ (ppm)=9.06~8.99 (CH, H), 8.92~8.72 (CH, 2H), 8.02~7.99 (CH, 2H), 7.73~7.57 (CH, 3H), 5.71~5.60 (CH_2, 2H), 1.51~1.42 (CH_3, 3H). ^{13}C NMR (75.5 MHz, D_2O) (Fig. S3B): δ (ppm)=149.75, 149.36, 146.87, 146.51, 138.92, 137.20, 136.41, 132.32, 130.45, 126.16, 124.98, 124.09, 60.08, 16.22. Elemental analysis: Found: C, 55.57; H, 4.86; N, 9.17 wt%. Calcd. for $C_{14}H_{13}N_2Br\cdot(0.75H_2O)$: C, 55.55; H, 4.83; N, 9.25 wt%.

Preparation of Phen$^{\bullet+}$-PHPs, Phen$^{\bullet+}$-PHP-2Br and Phen-PHP-2

Phen$^{\bullet+}$-PHPs were prepared by the Heck reaction of VPOSS with iDBPhen. In a typical run, VPOSS (0.1 mmol, 0.0633 g) was dissolved in 5 mL dimethylformamide (DMF), and iDBPhen (0.2 mmol, 0.1052 g) was dispersed in 5 mL of DMF and 1 mL of water. Then, the mixture was transferred to a 25 mL Teflon-lined autoclave. At the same time, K_2CO_3 (1 mmol, 0.1382 g) dissolved in 0.5 mL of water was added into the mixture solution, followed by the addition of the catalyst $Pd(PPh_3)_4$ (0.01 mmol, 0.0116 g) with stirring for 30 min. Next, the Teflon-lined autoclave was statically placed in a 120°C constant temperature oven for 72 h. After reaction, the solid products

were recovered by filtration and thoroughly washed with DMF, tetrahydrofuran, deionized water and ethanol. The brown powder Phen$^{\bullet+}$-PHP-2 was obtained by drying in vacuum at 80°C for 12 h. A series of Phen$^{\bullet+}$-PHP-*x* were obtained by varying the ratios of iDBPhen to VPOSS (*x*=1, 2, 4).

Further, bromide anion-paired Phen$^{\bullet+}$-PHP-2Br was prepared by post-treatment of the typical sample Phen$^{\bullet+}$-PHP-2 in 1 M HBr aqueous solution with stirring at room temperature for 12 h. After treatment, the mixture was filtered and washed thoroughly with deionized water. The targeted material Phen$^{\bullet+}$-PHP-2Br was obtained after drying in vacuum at 80^{o}C for 12 h. Besides, a control neutral phenanthroline-based porous hybrid polymer (Phen-PHP-2, Scheme S2) was prepared in a similar process using a suitable molar ratio (1:2) of VPOSS to DBPhen.

Catalytic tests

(1) Oxidation of sulfides

In a typical run, the model substrate methyl phenyl sulfide (1 mmol), the catalyst Phen$^{\bullet+}$-PHP-2 (20 mg), 30wt% H_2O_2 (2 mmol, 200 μL) and the solvent MeOH (4 mL) were successively added into in a 25 mL glass reaction tube. The reaction was carried out at 40 °C in a metal bath in the metal module with magnetic stirring for 1 h. After reaction, the solid catalyst was separated by centrifugation and the remaining solution was concentrated under reduced pressure. At last, the crude product was analyzed by ^{1}H NMR spectroscopy using $CDCl_3$ as solvent to determine the yield of the product phenyl methyl sulfoxide by comparison of the integrals of characteristic protons in the substrate and product (*Green Chem*., 2015, **17**, 1559-1571). The recovered catalyst was used for the next run.

(2) The catalytic CO_2 fixation reactions with epoxides

Typically, the model substrate epichlorohydrin (2 mmol) and the catalyst Phen$^{\bullet+}$-PHP-2Br (0.04 g) were added into placed in a 25 mL Schlenk tube connected with a CO_2 balloon (0.1 MPa). Then the mixture was stirred at the targeted temperature for a desired time. After reaction, 5 mL ethyl acetate was added into the reaction system and then the mixture was stirred for 0.5 h. Subsequently, the solid catalyst was separated by centrifugation, and the remaining solution was analyzed by gas chromatography (GC) using *n*-dodecane as an internal standard as well as ^{1}H NMR spectroscopy. For other substrates, the crude products were obtained by concentrating under reduced pressure at relative low temperatures and then were directly analyzed by ^{1}H NMR spectra using $CDCl_3$ as solvent to determine the yields of cyclic carbonates by comparison of the integrals of characteristic protons in the epoxide substrate and the cyclic carbonate product (*Green Chem*., 2016, **18**, 3116-3123). For recycling tests, the catalyst was recovered by centrifugation, washed with ethyl acetate for several times, dried, and used for the next run.

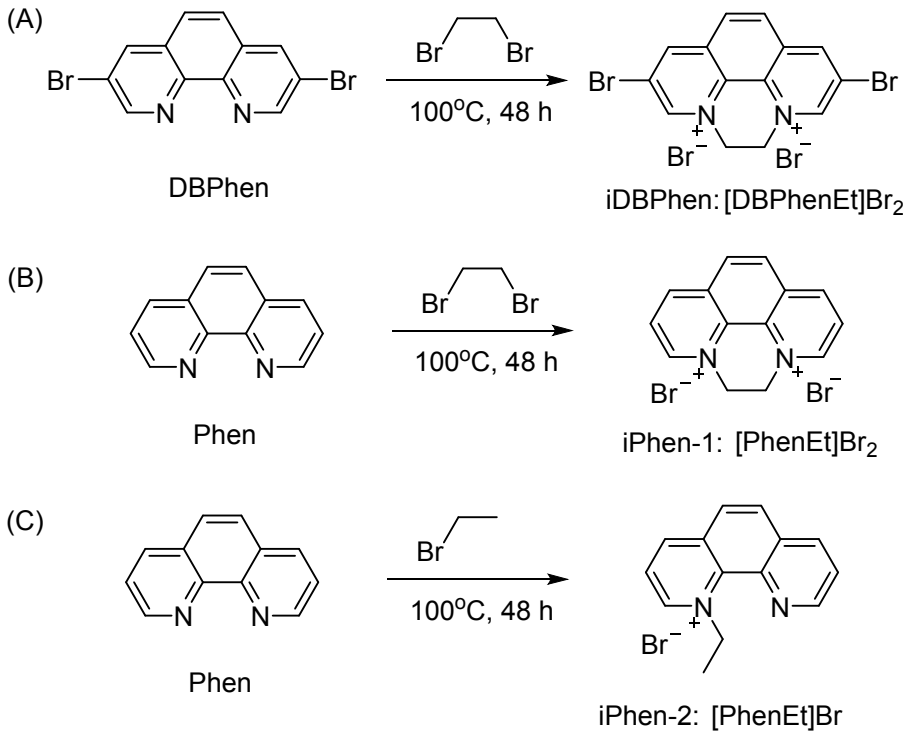

Scheme S1 Synthesis of phenanthroline-based ionic monomers (A) iDBPhen, (B) iPhen-1 and (C) iPhen-2 by one-step quaternization reactions of 3,8-dibromo-1,10-phenanthroline (DBPhen) or 1,10-phenanthroline (Phen) with 1,2-dibromoethane or bromoethane.

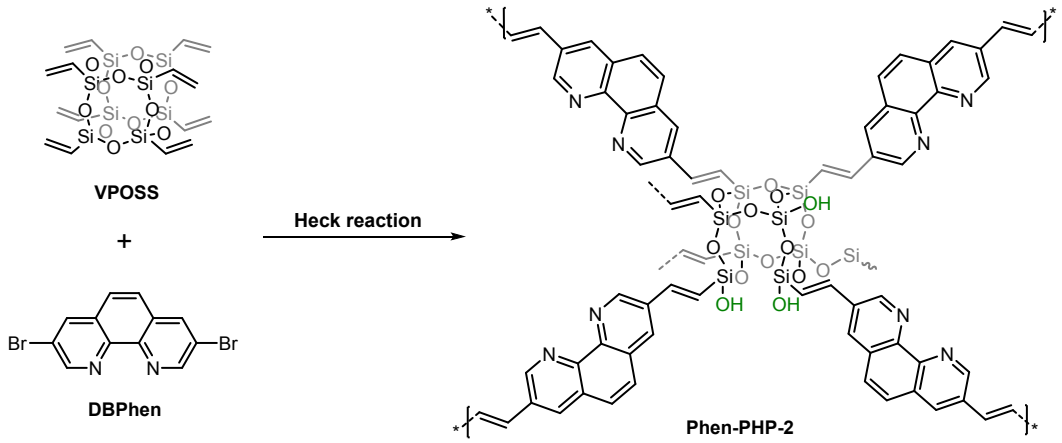

Scheme S2 Synthesis of a control neutral phenanthroline-based porous hybrid polymer (Phen-PHP-2) by the Heck reaction of VPOSS with DBPhen. Reaction condition: VPOSS (0.1 mmol), DBPhen (0.2 mmol), $Pd(PPh_3)_4$ (0.01 mmol), K_2CO_3 (1 mmol), DMF/H_2O, 120°C, 72 h.

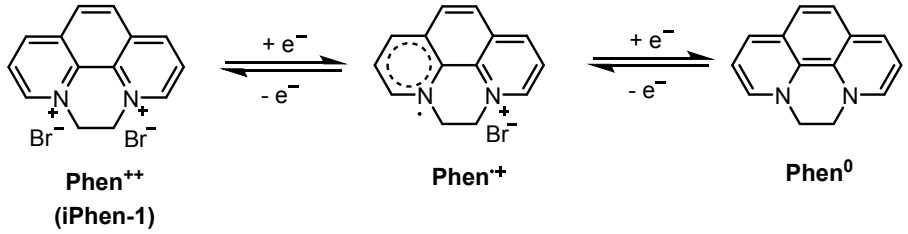

Scheme S3 Two plausible reversible redox states (a radical cationic Phen specie Phen $N^{\bullet+}$ and reduced neutral $Phen^0$) of phenanthroline ionic monomer iPhen-1 ($Phen^{++}$).

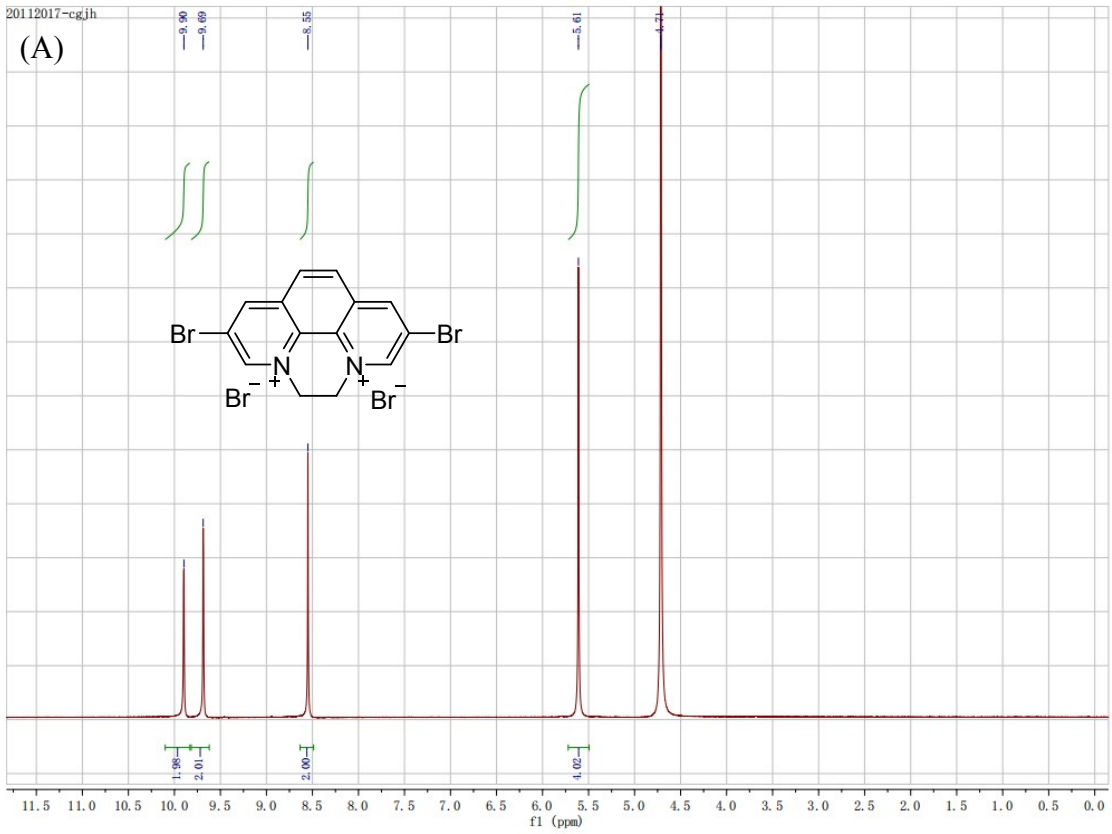

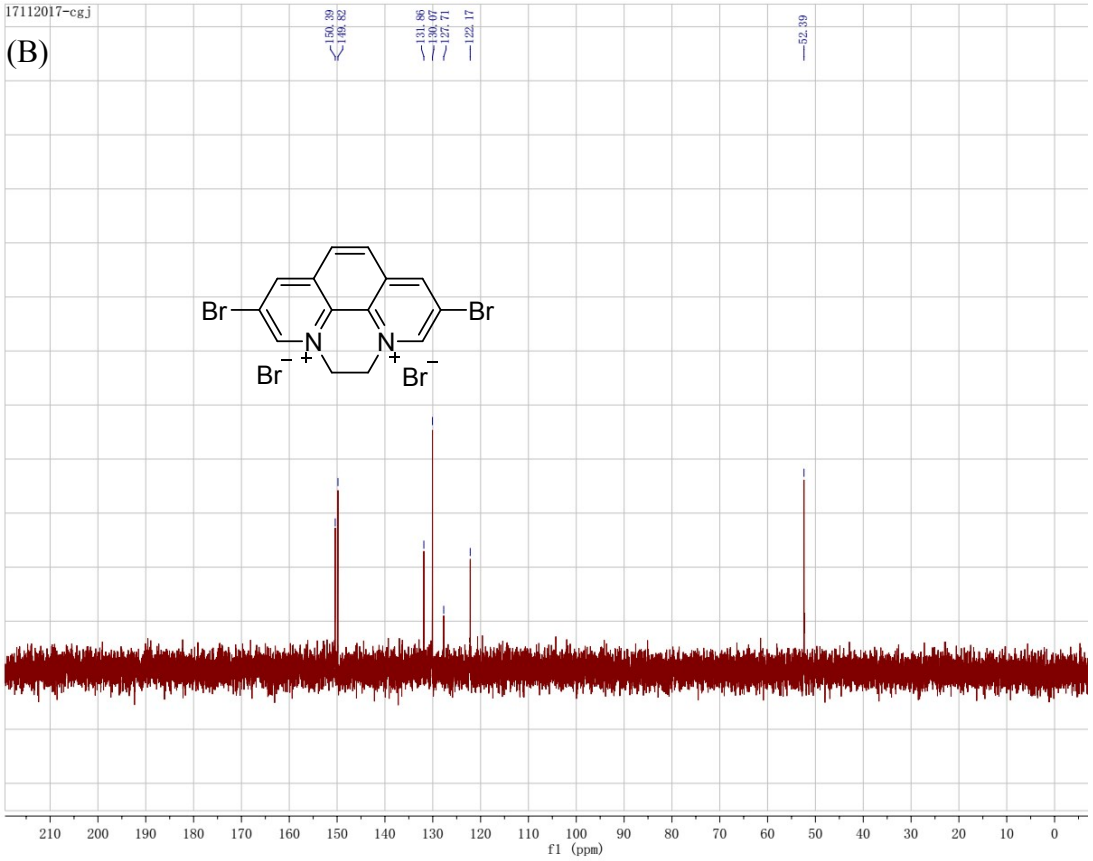

Fig. S1 (A) ^{1}H NMR and (B) ^{13}C NMR of $[DBPhenEt]Br_2$ using D_2O as the solvent.

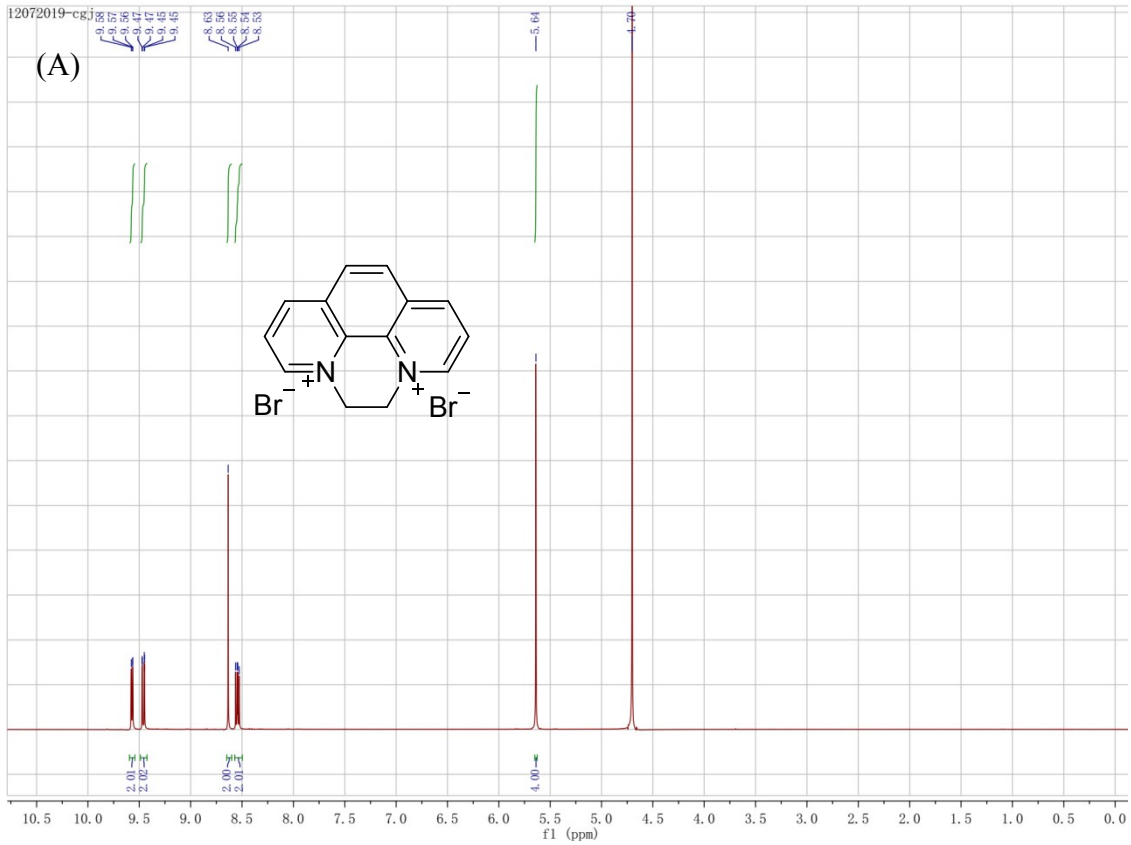

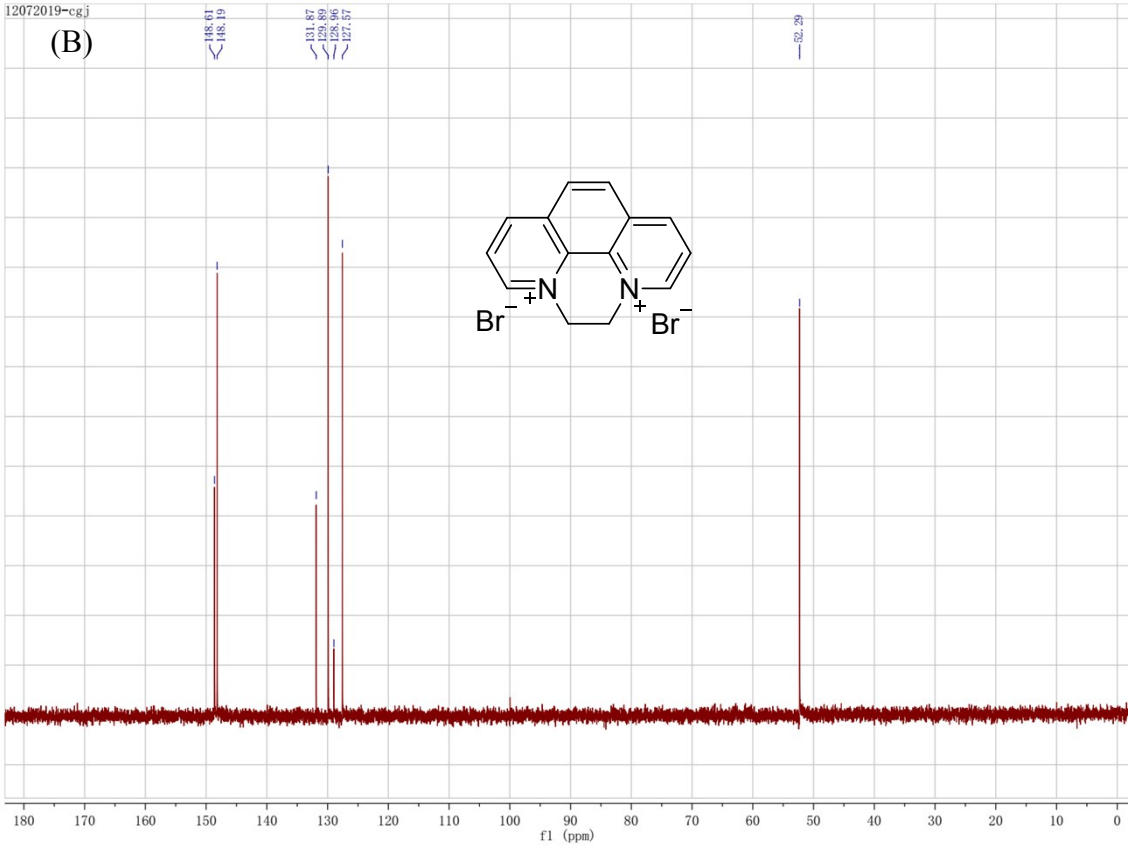

Fig. S2 (A) ^{1}H NMR and (B) ^{13}C NMR of iPhen-1: [PhenEt]Br_2 using D_2O as the solvent.

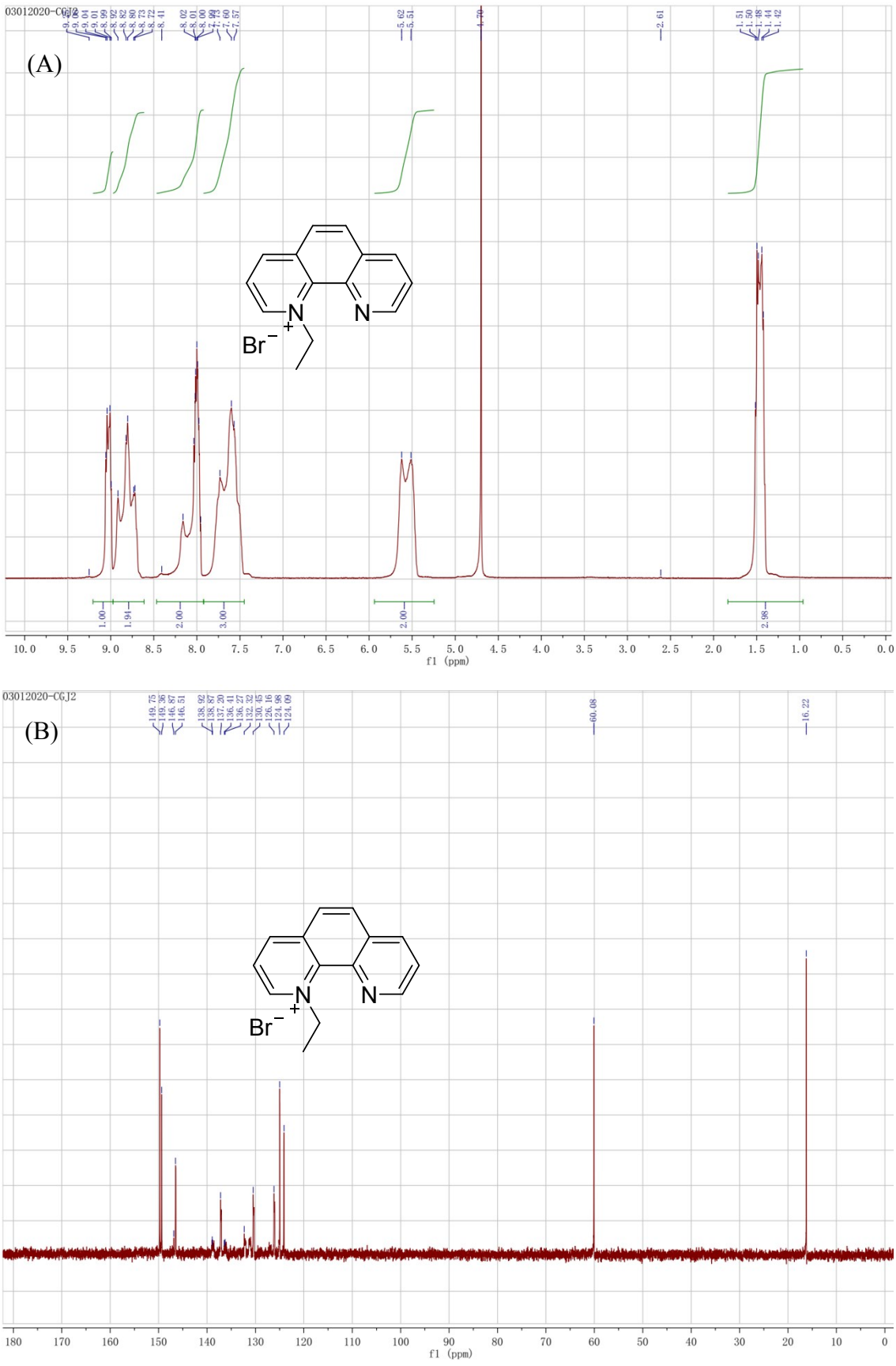

Fig. S3 (A) ^{1}H NMR and (B) ^{13}C NMR of iPhen-2: [PhenEt]Br using D_2O as the solvent.

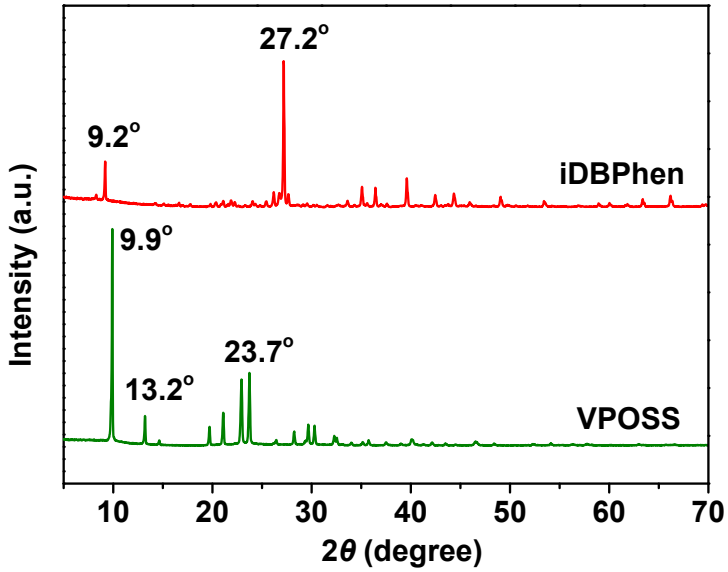

Fig. S4 XRD pattern of the ionic monomer iDBPhen and VPOSS monomer.

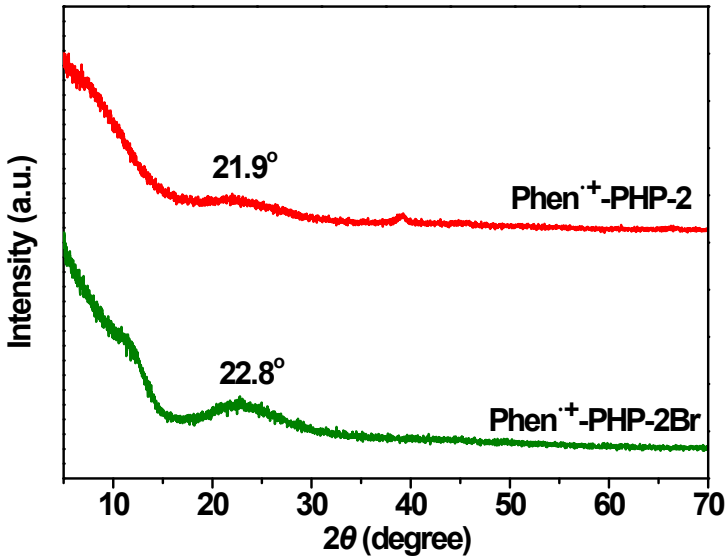

Fig. S5 XRD pattern of the typical sample Phen$^{\bullet+}$-PHP-2 and Phen$^{\bullet+}$-PHP-2Br.

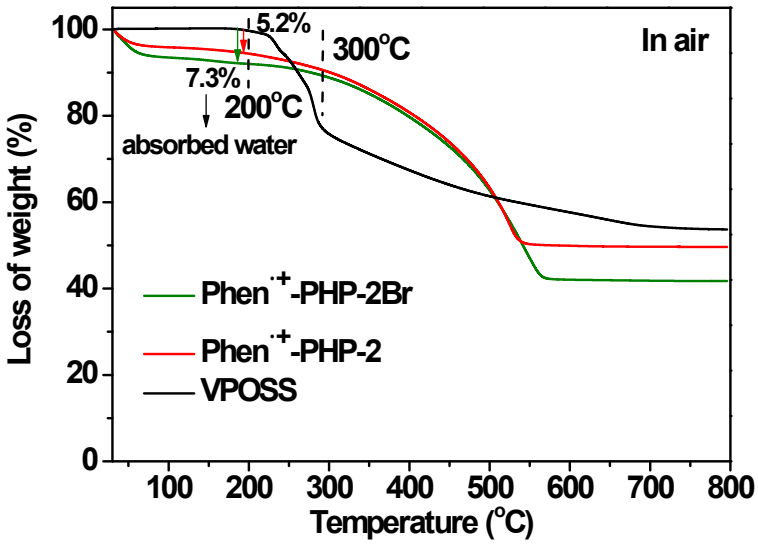

Fig. S6 Thermogravimetric analysis (TGA) curves of Phen$^{\bullet+}$-PHP-2, Phen$^{\bullet+}$-PHP-2Br and VPOSS under air atmosphere.

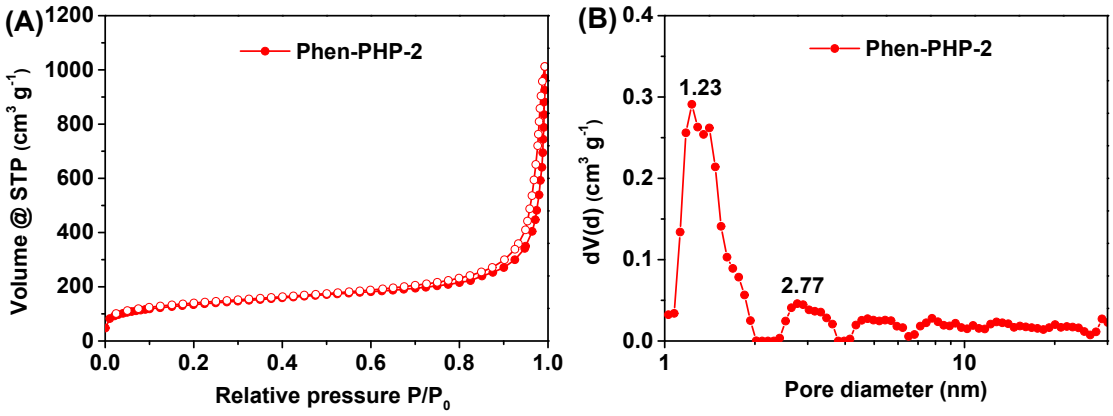

Fig. S7 (A) N_2 adsorption-desorption isotherm and (B) NLDFT pore size distribution of Phen-PHP-2.

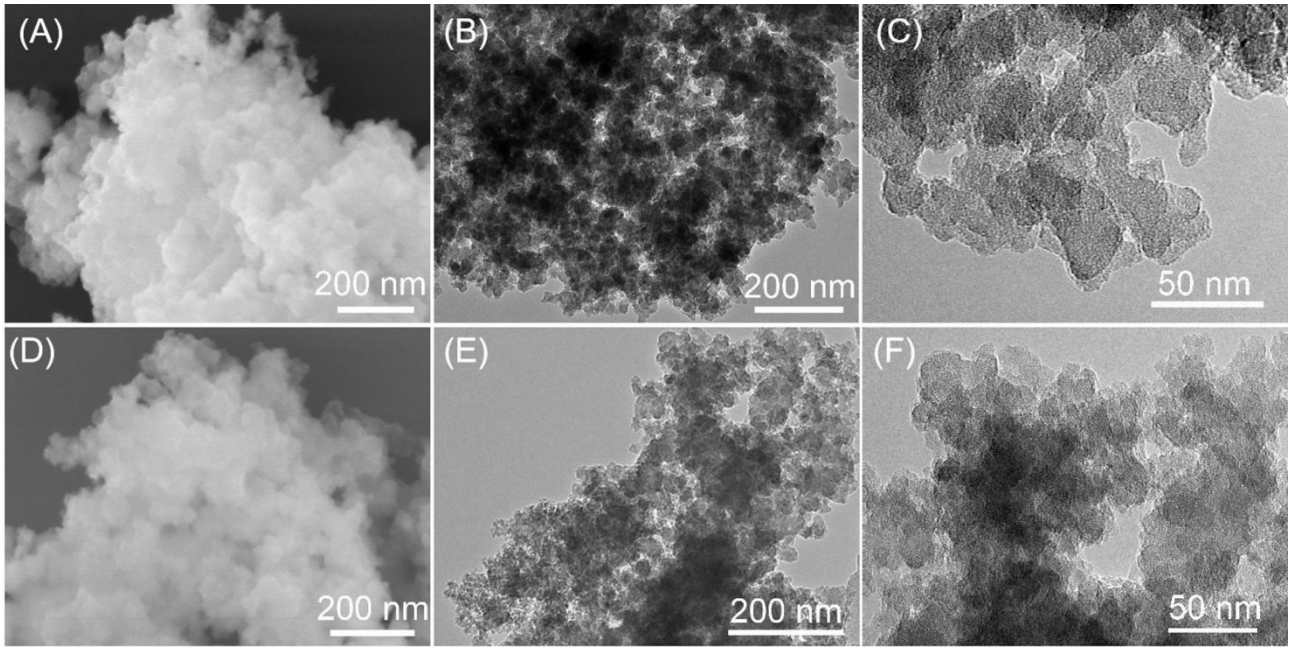

Fig. S8 SEM and TEM images of (A, B and C) Phen$^{\bullet+}$-PHP-2 and (D, E and F) Phen$^{\bullet+}$-PHP-2Br.

Table S1 Catalytic oxidation of methyl phenyl sulfide with H_2O_2 over various metal-based heterogeneous catalysts.

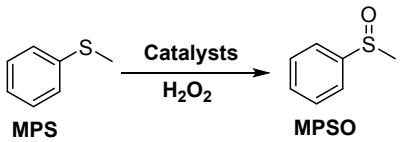

Catalysts	Reaction Conditions	MPSO Yield (%)	Ref.
$[C_4mim]_3PM$	H_2O_2, CH_3OH, rt, 30 min	97.2	S1
Nb@OC@[TBA][LA]	H_2O_2, CH_3OH, 0 °C, 40 min	96	S2
$PVPyPS_4PMo_{10}V_2$	H_2O_2, EtOH, rt, 10 min	97	S3
Fe_3O_4@S-ABENZ@VO	H_2O_2, rt, 80 min	97	S4
MNP@TA-IL/W	H_2O_2, H_2O, 25 °C, 1 h	97	S5
PMATi	H_2O_2, H_2O, rt, 1 h	97	S6
PAMAM-G1-PMo	H_2O_2, CH_3OH, 30 °C, 4 h	90	S7
$Phen^{\bullet+}$-PHP-2	**H_2O_2, CH_3OH, 40 °C, 1 h**	**99**	**This work**

Table S2 The detailed comparisons of catalytic activities in the conversion of CO_2 with ECH over metal-free porous ionic polymers (PIPs) and PIPs with HBD groups.[#]

Catalysts	*P* (MPa)	*T* (°C)	*t* (h)	Yield (%)	Ref.
PCP-Cl	3	100	12	98	S8
IT-POP-1	1	120	10	99	S9
POM3-IM	1	120	8	90	S10
cCTF-500	1	90	12	95	S11
CCTF-350	0.1	120	24	93.1	S12
PDMBr	0.1	120	12	91.3	S13
PIP-Bn-Cl	0.1	100	3	99	S14
COP-222	0.1	100	24	99	S15
PDBA-Cl-SCD	0.1	90	6	99.3	S16
HIP-Br-2	0.1	70	96	90	S17
VIP-Br	0.1	60	48	99	S18
FIP-Im	1	80	10	99	S19
PQPBr-2OH	0.5	120	4	99	S20
PGDBr-5-2OH	0.1	70	24	91	S21
V-PCIF-Br	0.1	80	72	97	S22
V-iPHP-1	0.1	60	72	99	S23
IM-iPHP-2	0.1	60	72	99	S24
PPS-mOH-Bn	0.1	50	72	78	S25
POF-PNA-Br	0.1	40	48	94.1	S26
IMIN-Br-OH	0.1	60	48	99	S27
Phen$^{\bullet+}$-PHP-2Br	**0.1**	**60/40**	**48/96**	**99/93**	**This work**

[#] It was worth pointing out that different catalysts were evaluated under different reaction conditions (such as reaction temperature and time, CO_2 pressure and the amount of substrate/catalyst). Therefore, it is difficult to fairly compare their catalytic activities between different systems. The above listed catalytic activities in terms of their final yields should be considered in a reasonable comparison. The green highlighted catalysts represent PIPs with HBD groups.

^{1}H NMR spectra and data for the crude sulfoxides

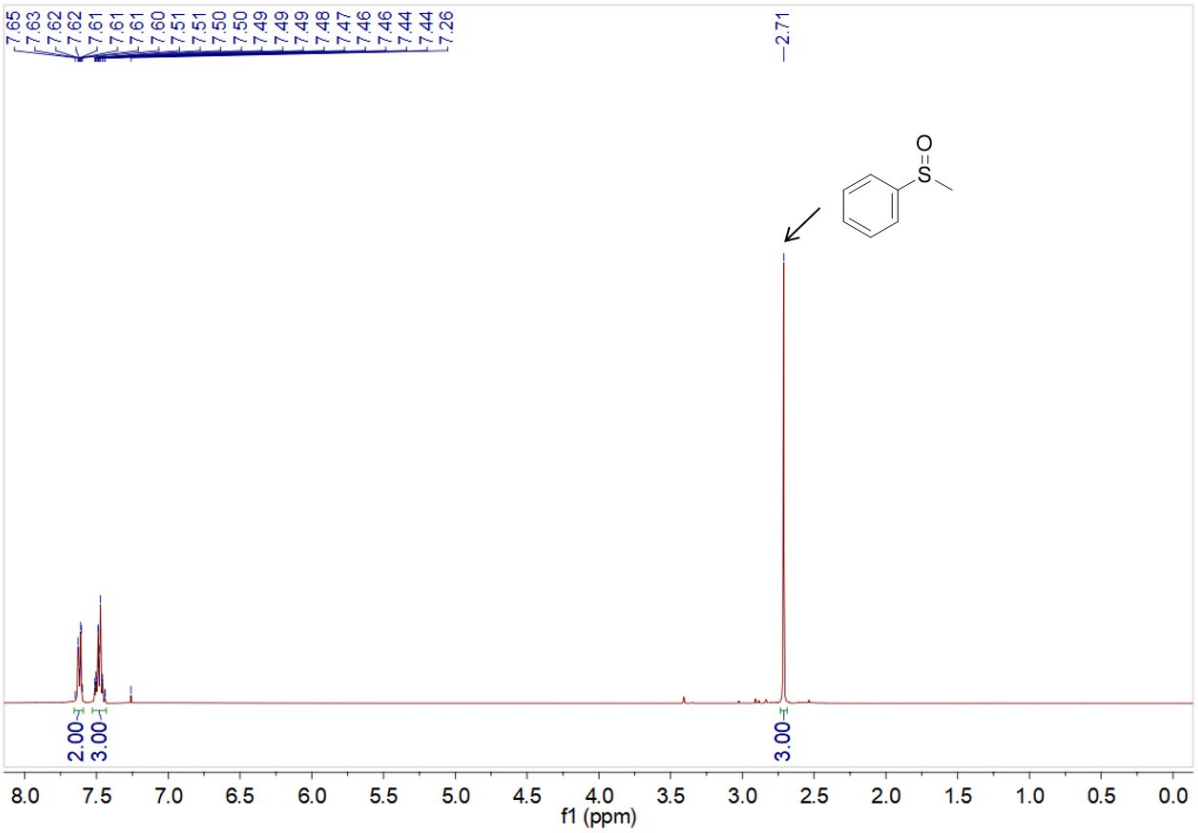

Fig. S9 ^{1}H NMR spectrum of phenyl methyl sulfoxide (400 MHz, $CDCl_3$): δ=7.66~7.59 (m, 2H), 7.53~7.43 (m, 3H), 2.71 ppm (s, 3H).

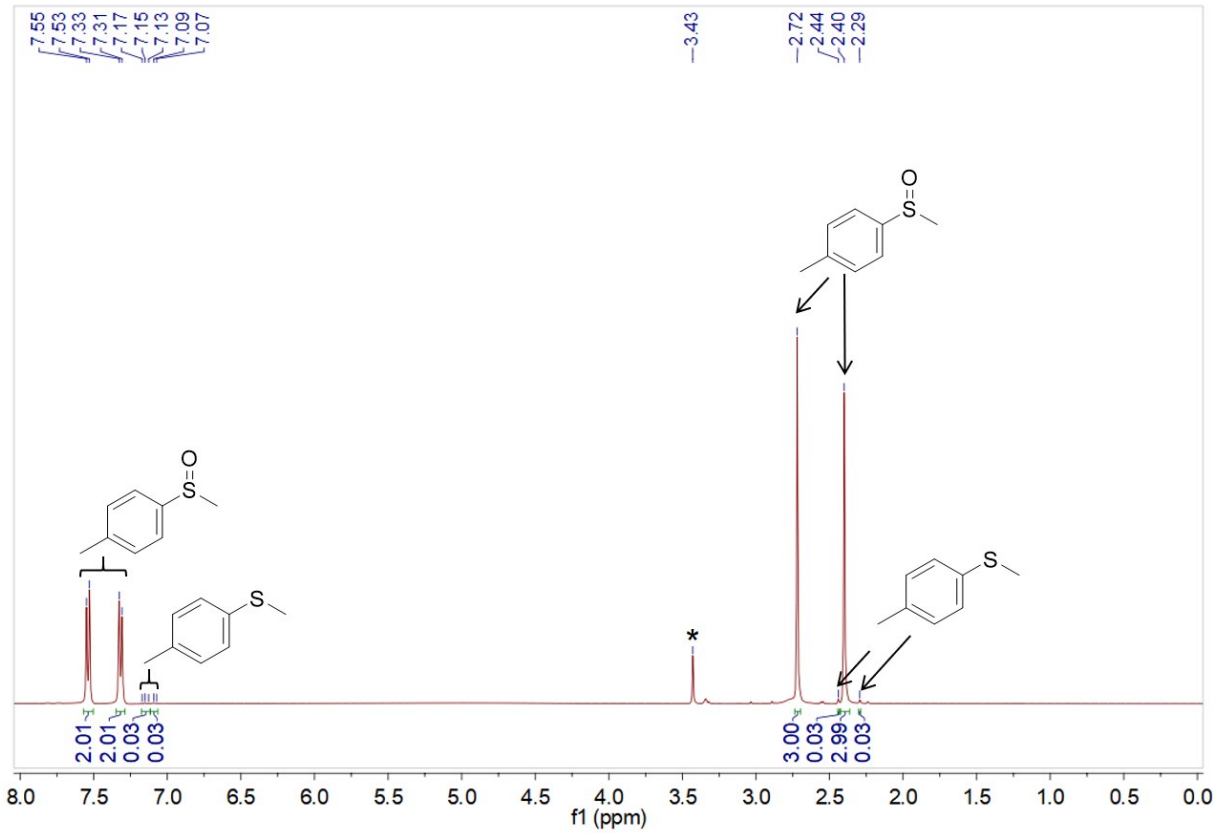

Fig. S10 ^{1}H NMR spectrum of methyl *p*-tolyl sulfoxide (400 MHz, $CDCl_3$): δ=7.54 (m, 2H), 7.32 (m, 2H), 2.72 (s, 3H), 2.40 ppm (s, 3H). * represents the residual solvent MeOH.

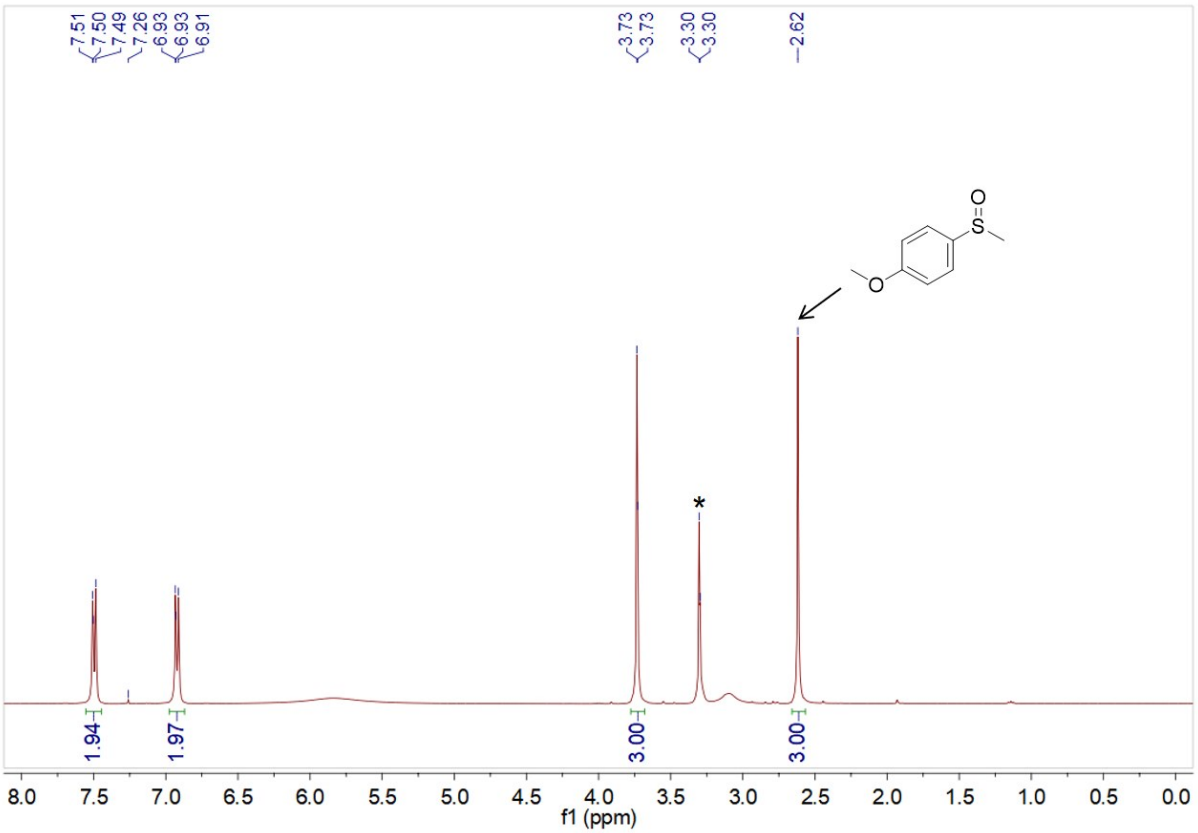

Fig. S11 ^{1}H NMR spectrum of 4-methoxyphenyl methyl sulfoxide (400 MHz, $CDCl_3$): δ=7.55~7.45 (m, 2H), 6.98~6.87 (m, 2H), 3.73 (m, 3H), 2.62 ppm (s, 3H). * represents the residual solvent MeOH.

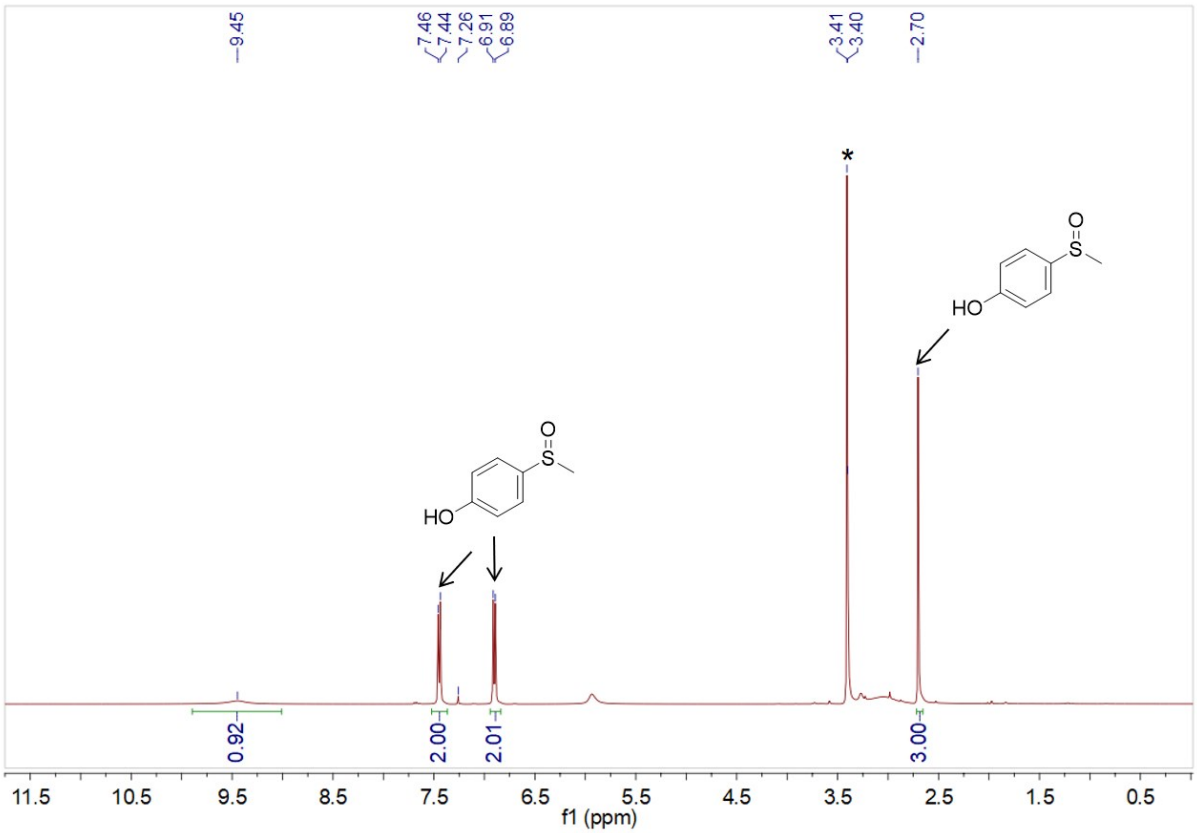

Fig. S12 ^{1}H NMR spectrum of 4-(methylsulfinyl)phenol (400 MHz, $CDCl_3$): δ=9.45 (s, 1H), 7.46~7.44 (m, 2H), 6.91~6.89 (m, 2H), 2.70 ppm (s, 3H). * represents the residual solvent MeOH.

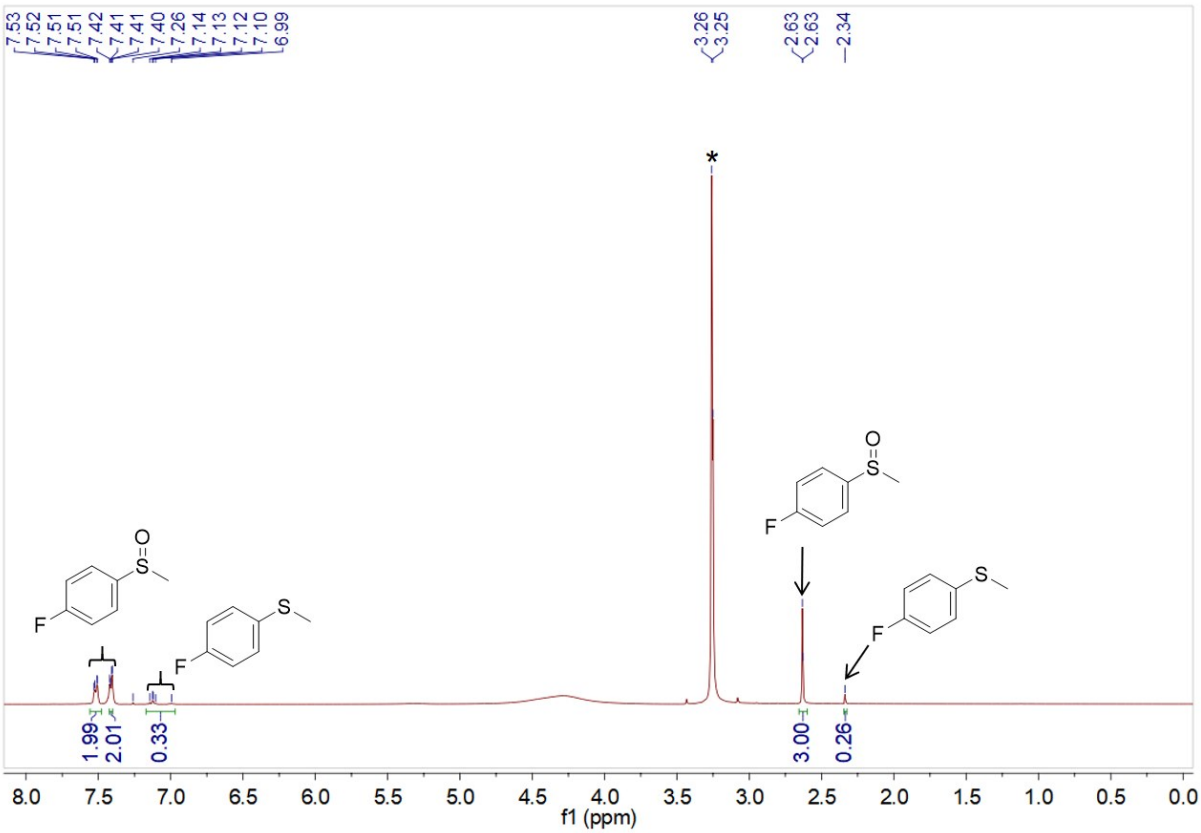

Fig. S13 ^{1}H NMR spectrum of 1-fluoro-4-(methylsulfinyl)benzene (400 MHz, $CDCl_3$): δ=7.52 (m, 2H), 7.41 (m, 2H), 2.63 ppm (s, 3H). * represents the residual solvent MeOH.

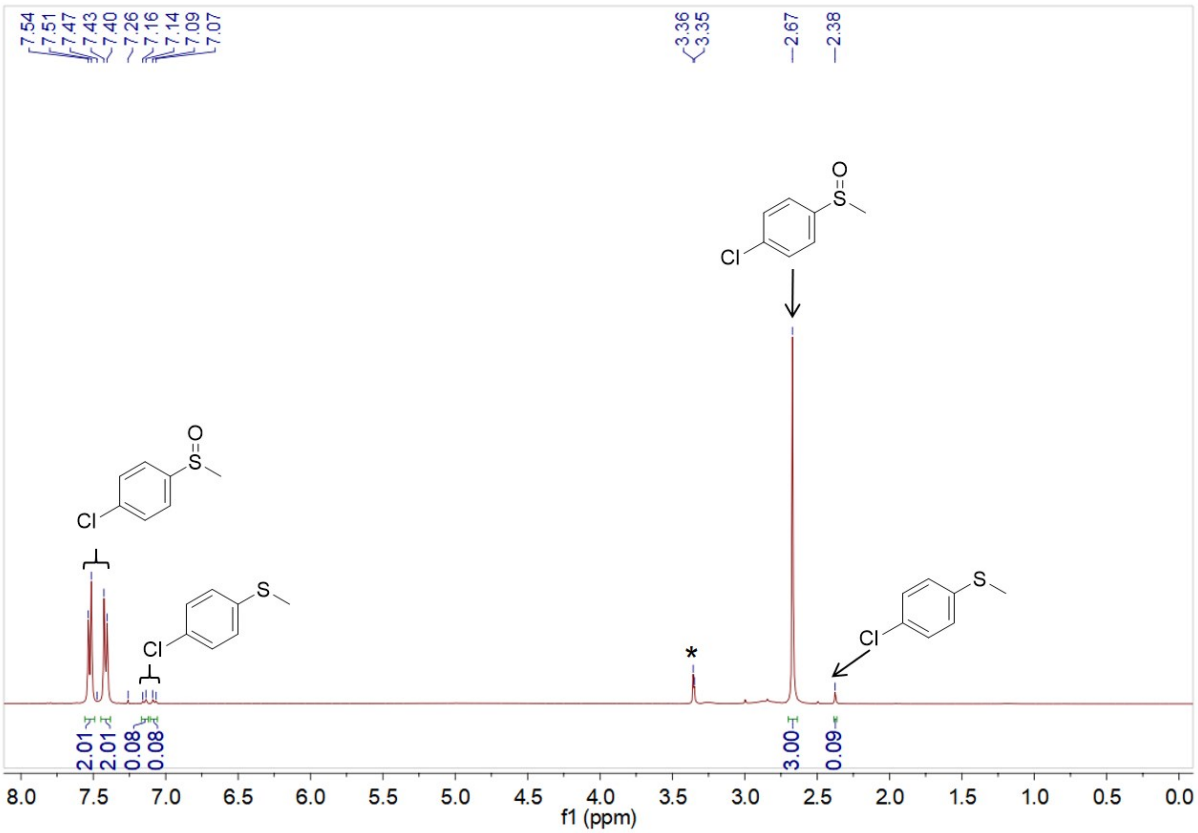

Fig. S14 ^{1}H NMR spectrum of 1-chloro-4-(methylsulfinyl)benzene (400 MHz, $CDCl_3$): δ=7.52 (m, 2H), 7.42 (m, 2H), 2.67 ppm (s, 3H). * represents the residual solvent MeOH.

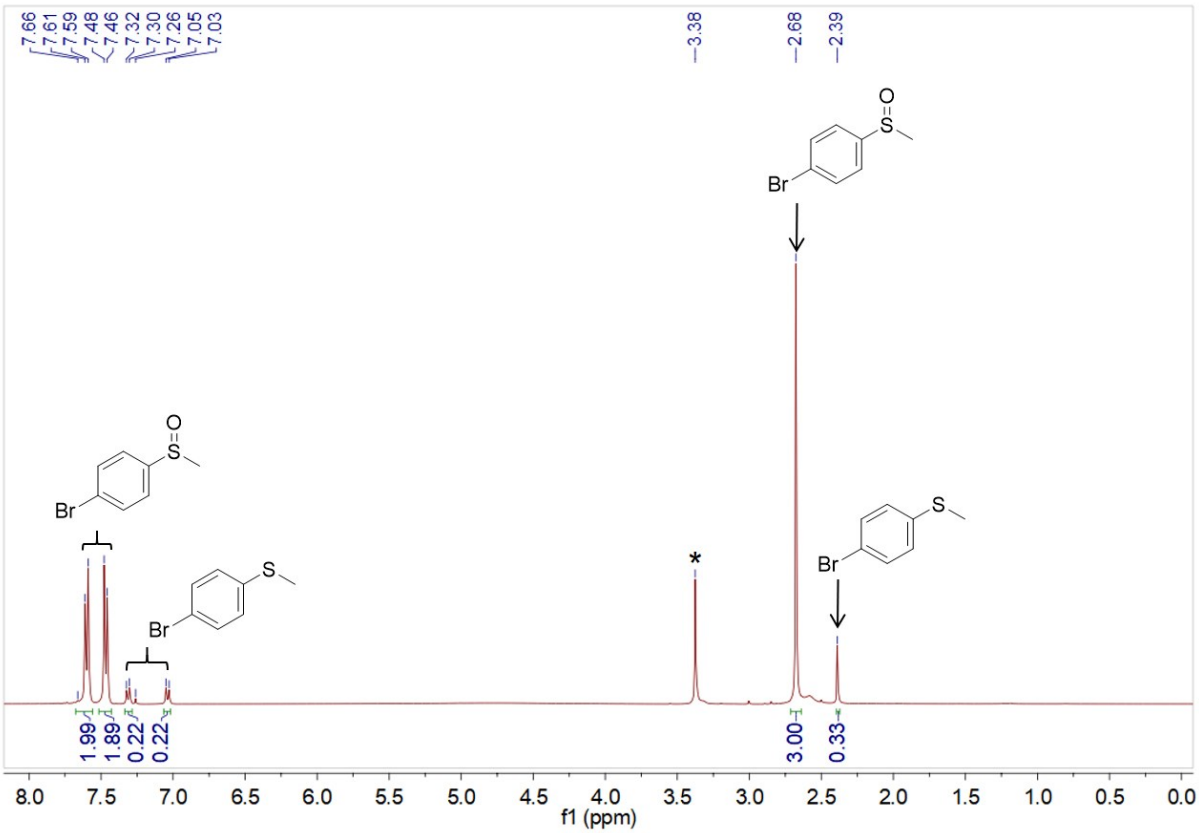

Fig. S15 ^{1}H NMR spectrum of 1-bromo-4-methylsulfinylbenzene (400 MHz, $CDCl_3$): δ=7.68~7.56 (m, 2H), 7.47 (m, 2H), 2.68 ppm (s, 3H). * represents the residual solvent MeOH.

^{1}H NMR data and spectra for the crude cyclic carbonates

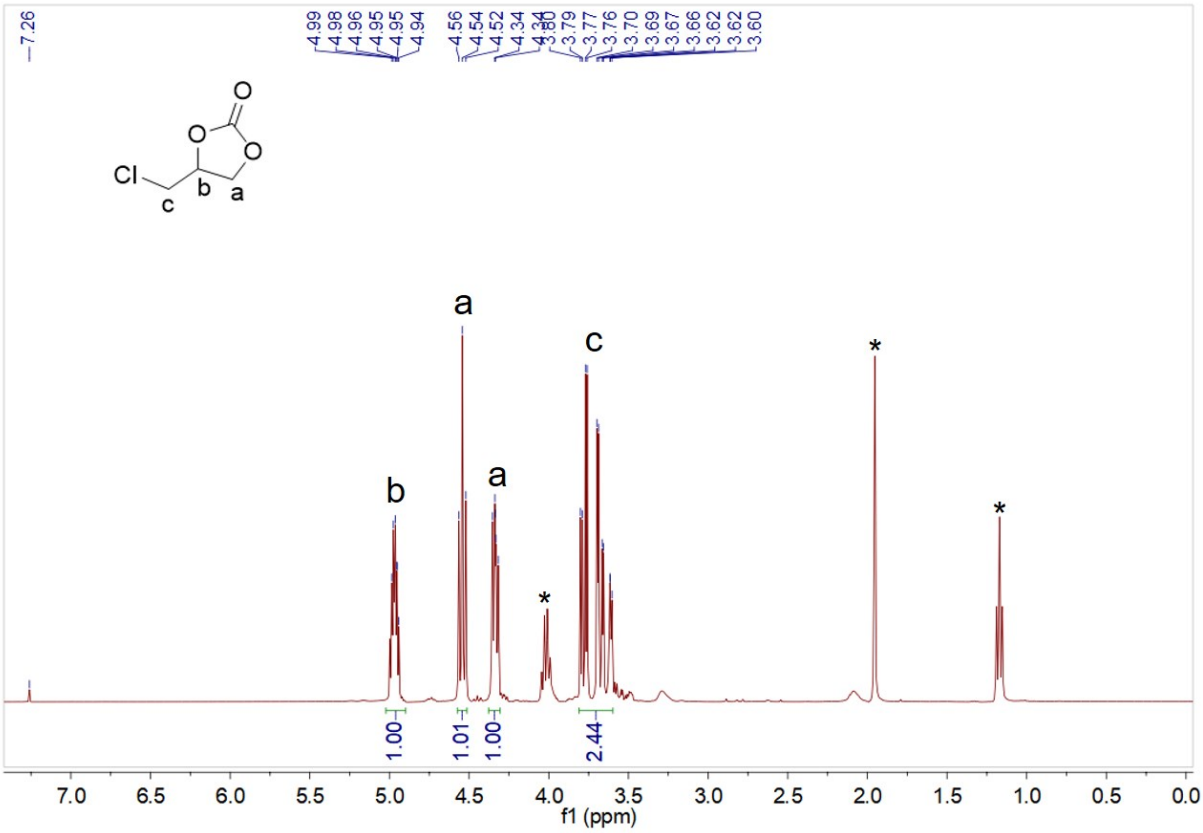

Fig. S16 ^{1}H NMR spectrum of 4-(chloromethyl)-1,3-dioxolan-2-one (400 MHz, $CDCl_3$): δ=4.96 (1H, CH), 4.54 (1H, CH_2), 4.38~4.30 (1H, CH_2), 3.81~3.60 ppm (2H, CH_2). * represents the residual solvent ethyl acetate.

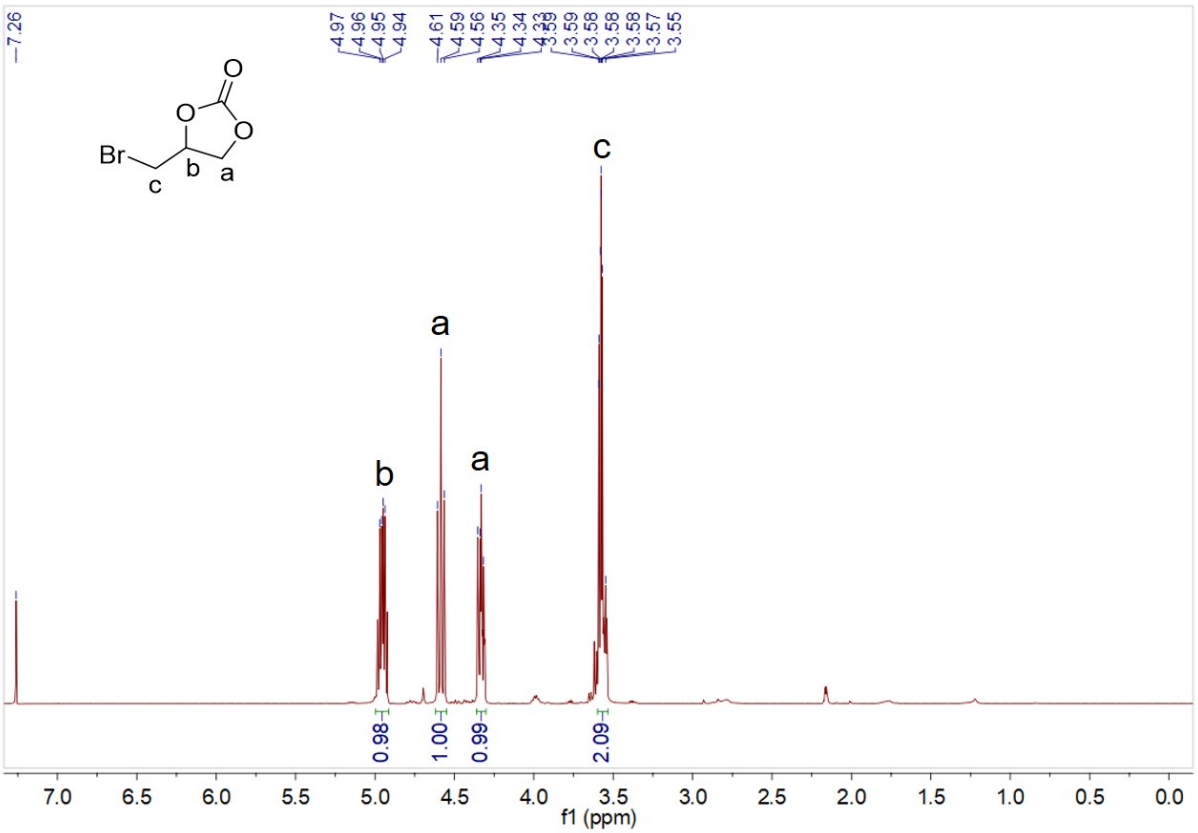

Fig. S17 ^{1}H NMR spectrum of 4-(bromomethyl)-1,3-dioxolan-2-one (400 MHz, $CDCl_3$): δ=4.95 (1H, CH), 4.59 (1H, CH_2), 4.33 (1H, CH_2), 3.60~3.53 ppm (2H, CH_2).

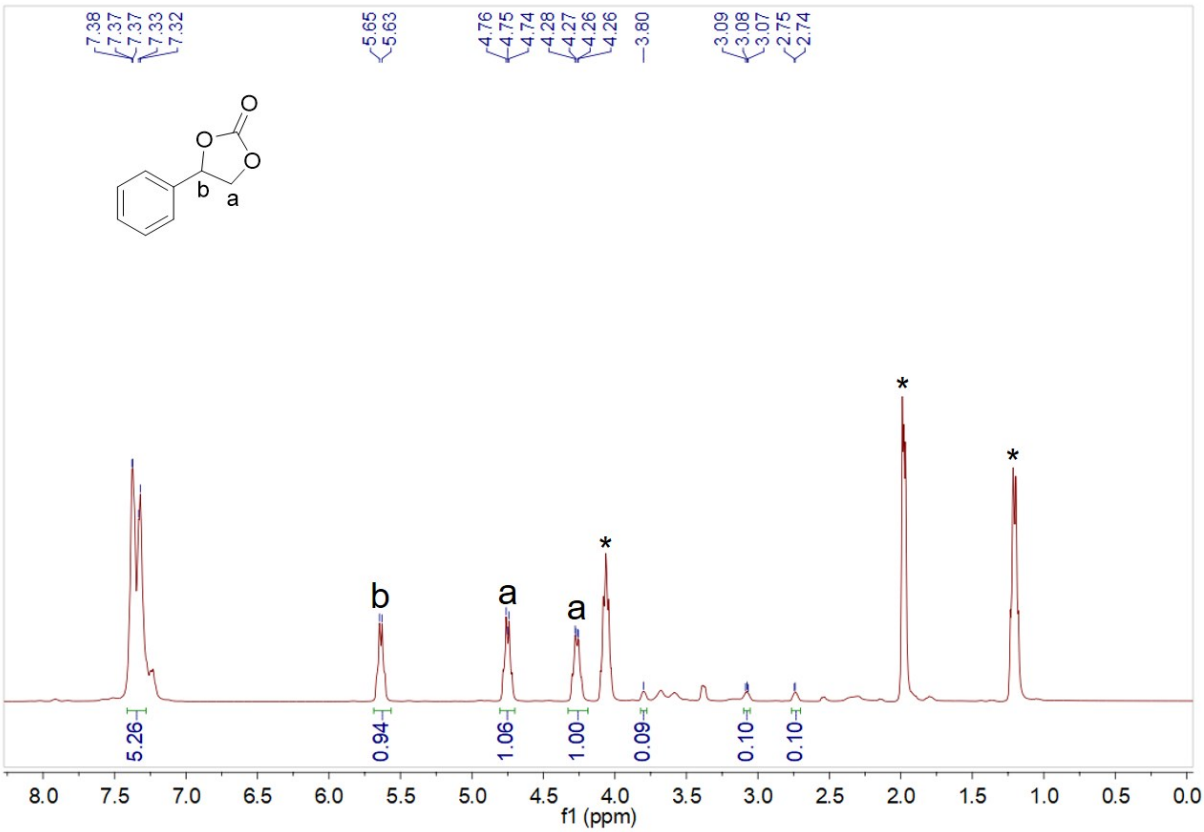

Fig. S18 ^{1}H NMR spectrum of 4-phenyl-1,3-dioxolan-2-one (400 MHz, $CDCl_3$): δ=7.41~7.28 (5H, CH), 5.64 (1H, CH_2), 4.81~4.70 (1H, CH_2), 4.27 ppm (1H, CH_2). * represents the residual solvent ethyl acetate.

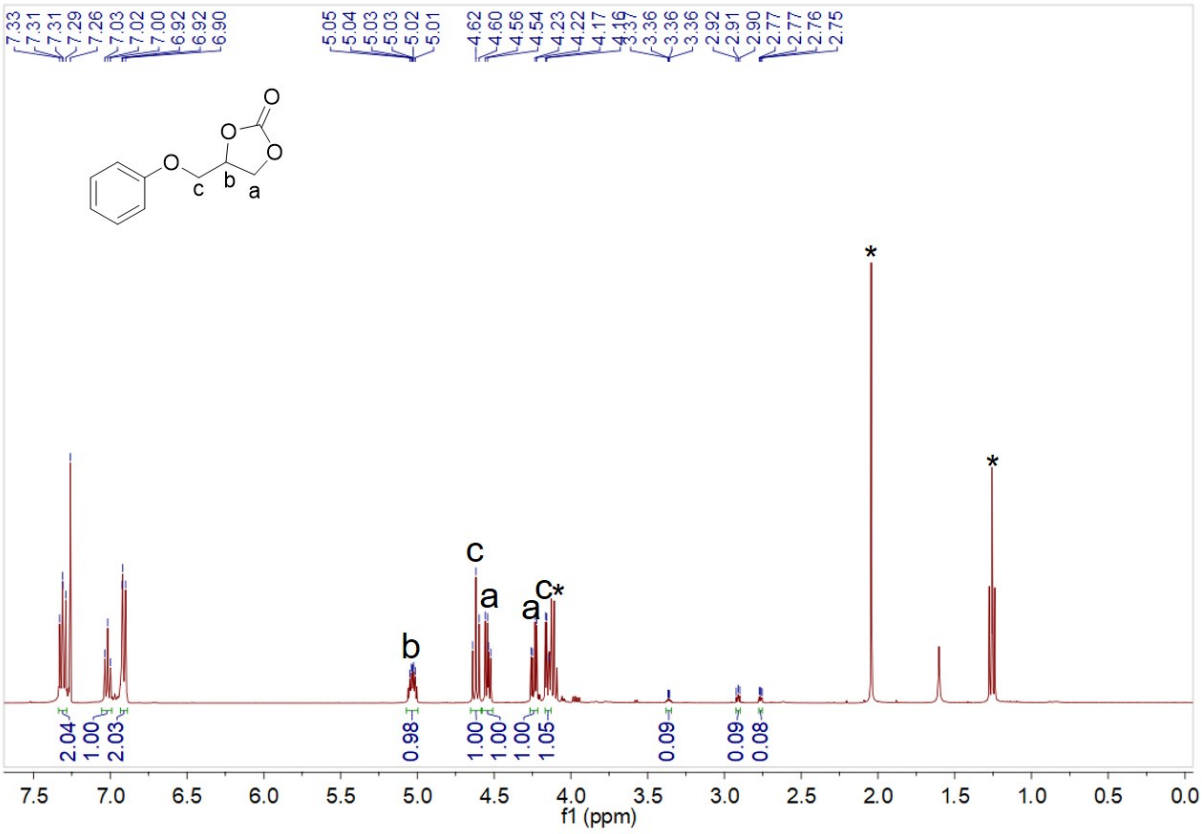

Fig. S19 ^{1}H NMR spectrum of 4-(phenoxymethyl)-1,3-dioxolan-2-one (400 MHz, $CDCl_3$): δ=7.31 (2H, CH), 7.02 (1H, CH), 6.93~6.89 (2H, CH), 5.07~5.00 (1H, CH), 4.62 (1H, CH_2), 4.54 (1H, CH_2), 4.24 (1H, CH_2), 4.17~4.13 ppm (1H, CH_2). * represents the residual solvent ethyl acetate.

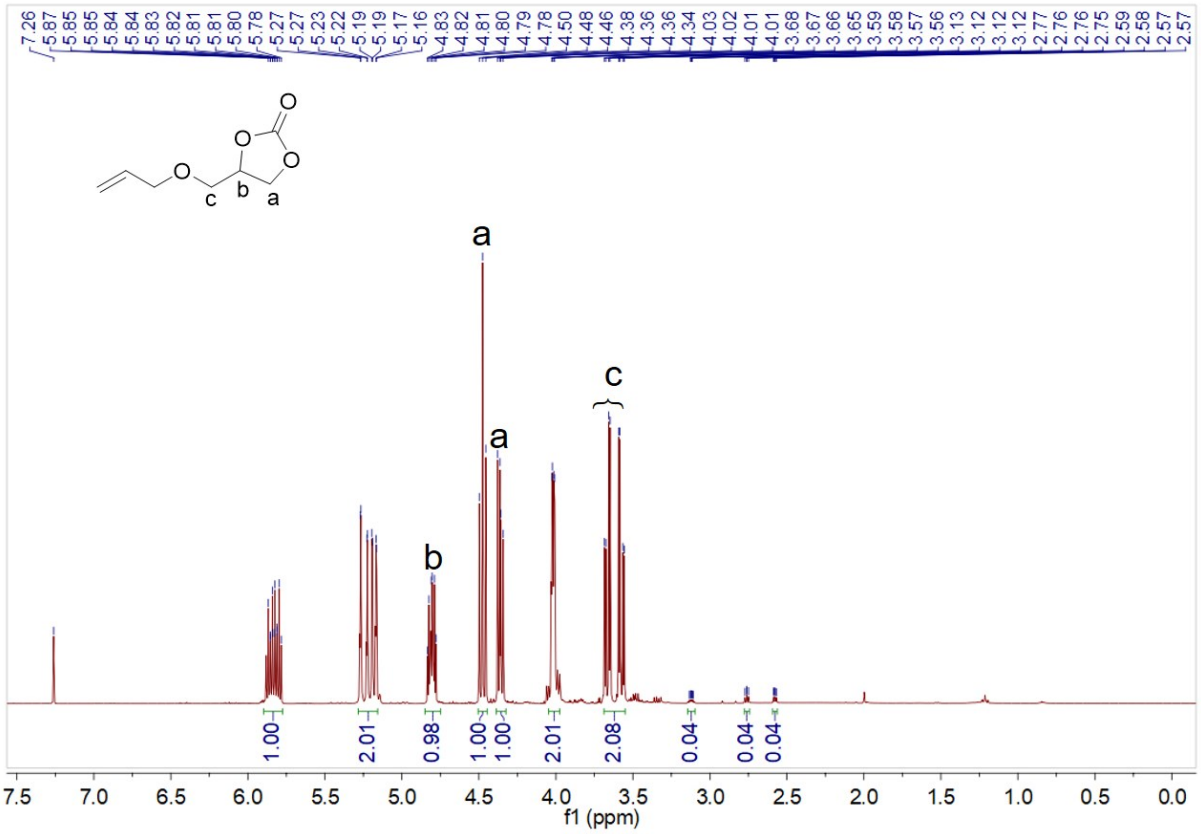

Fig. S20 ^{1}H NMR spectrum of allyloxymethyl-1,3-dioxolan-2-one (400 MHz, $CDCl_3$): δ=5.90~5.78 (1H, CH), 5.21 (2H, CH_2), 4.81 (1H, CH), 4.48 (1H, CH_2), 4.36 (1H, CH_2), 4.02 (2H, CH_2), 3.62 ppm (2H, CH_2).

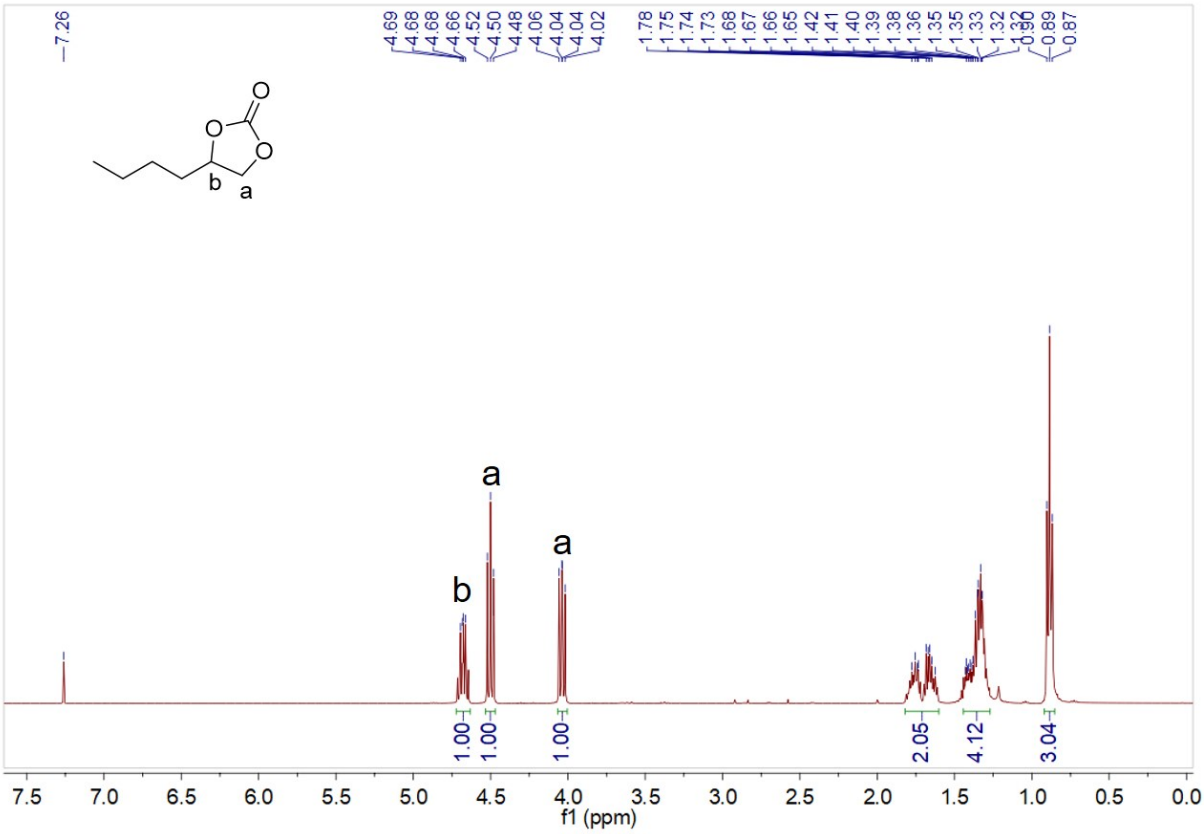

Fig. S21 ^{1}H NMR spectrum of 4-butyl-1,3-dioxolan-2-one (400 MHz, $CDCl_3$): δ=4.68 (1H, CH_2), 4.50 (1H, CH_2), 4.04 (1H, CH_2), 1.82~1.60 (2H, CH_2), 1.44~1.27 (4H, CH_2), 0.89 ppm (3H, CH_3).

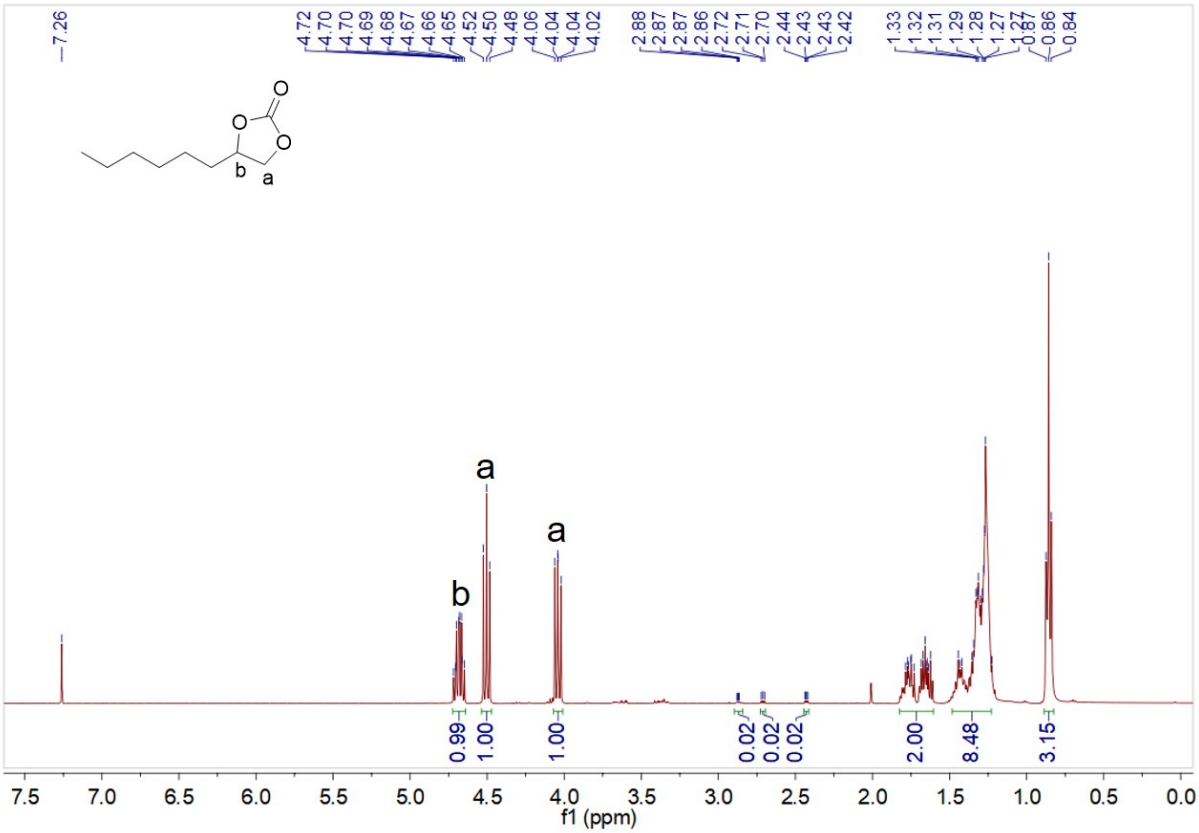

Fig. S22 ^{1}H NMR spectrum of 4-hexyl-1,3-dioxolan-2-one (400 MHz, $CDCl_3$): δ=4.68 (1H, CH_2), 4.54~4.47 (1H, CH_2), 4.04 (1H, CH_2), 1.83~1.60 (2H, CH_2), 1.48~1.23 (8H, CH_2), 0.86 ppm (3H, CH_3).

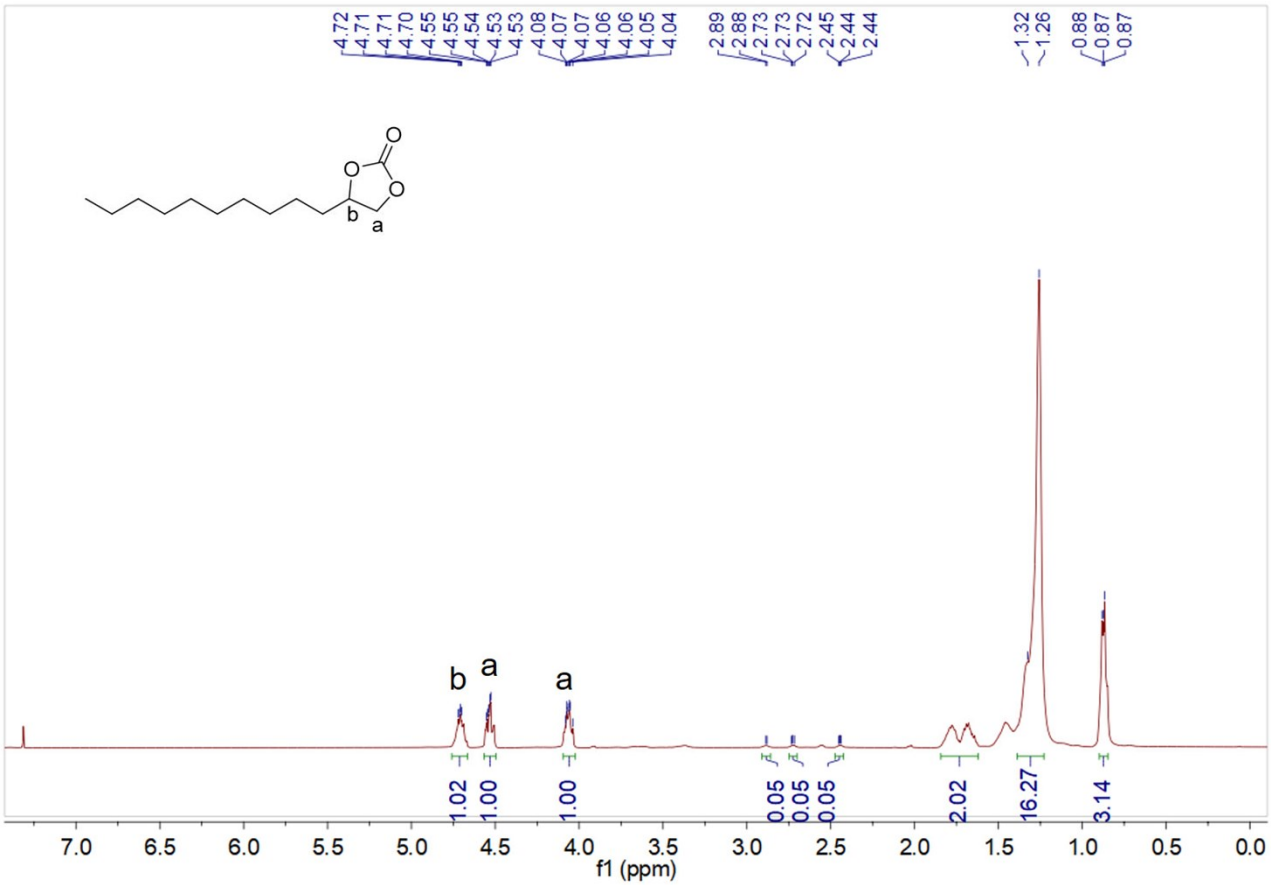

Fig. S23 ^{1}H NMR spectrum of 4-decyl-1,3-dioxolan-2-one (400 MHz, $CDCl_3$): δ=4.66 (1H, CH_2), 4.51~4.44 (1H, CH_2), 4.04~3.97 (1H, CH_2), 1.79~1.57 (2H, CH_2), 1.45~1.19 (16H, CH_2), 0.85~0.79 ppm (3H, CH_3).

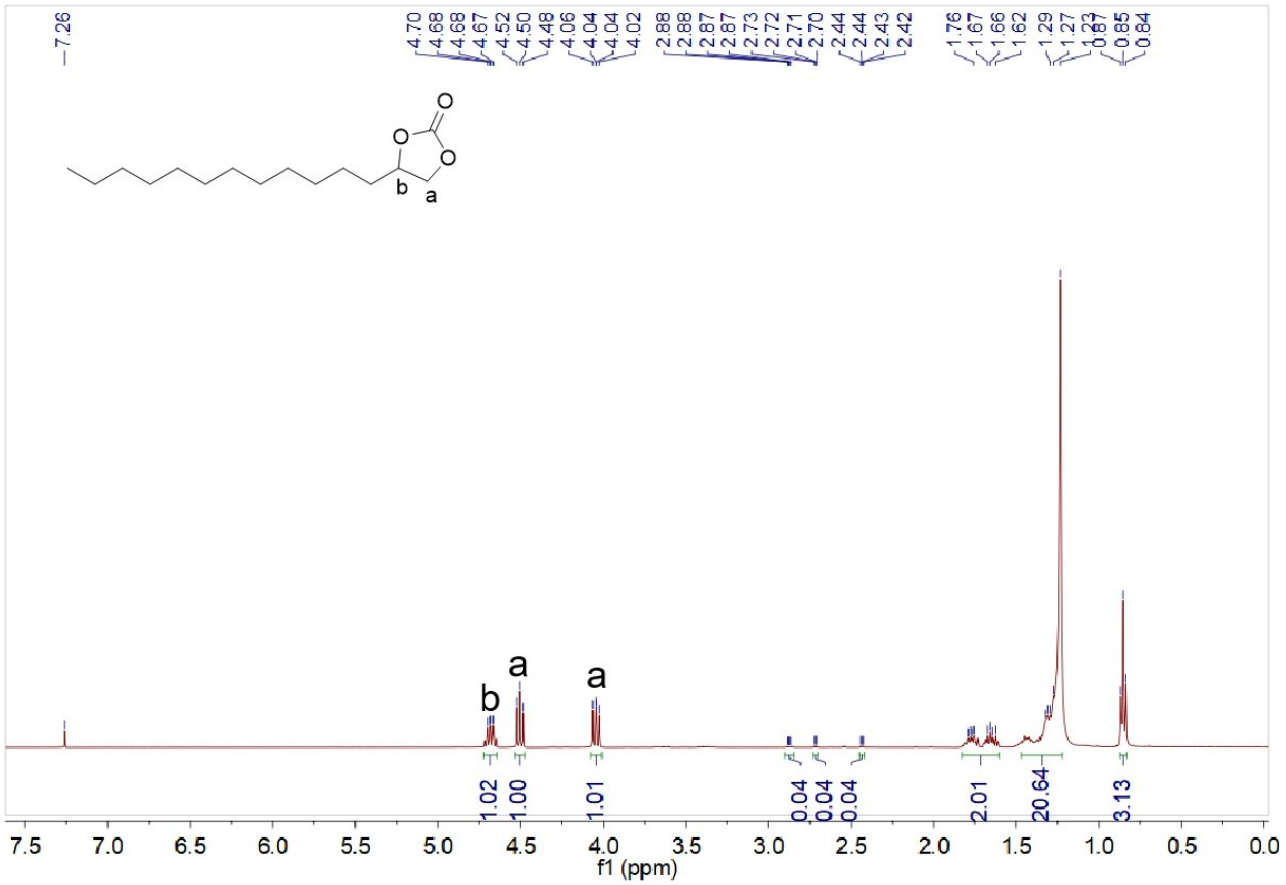

Fig. S24 ^{1}H NMR spectrum of 4-dodecyl-1,3-dioxolan-2-one (400 MHz, $CDCl_3$): δ=4.68 (1H, CH_2), 4.50 (1H, CH_2), 4.04 (1H, CH_2), 1.83~1.60 (2H, CH_2), 1.47~1.22 (20H, CH_2), 0.85 ppm (3H, CH_3).

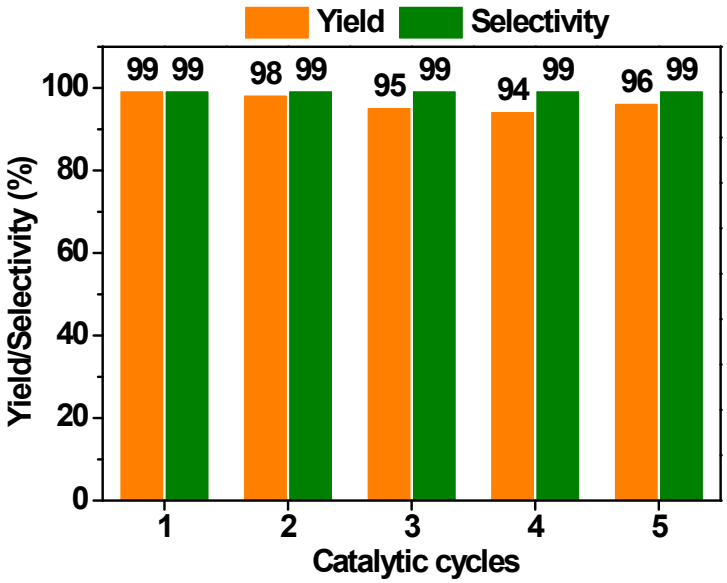

Fig. S25 A five-cycle assessment in the catalytic reusability of Phen$^{\bullet+}$-PHP-2Br for the CO_2 conversion with ECH. Reaction conditions: ECH (2 mmol), CO_2 pressure (0.1 MPa), the catalyst (40 mg), 60^{o}C, 48 h.

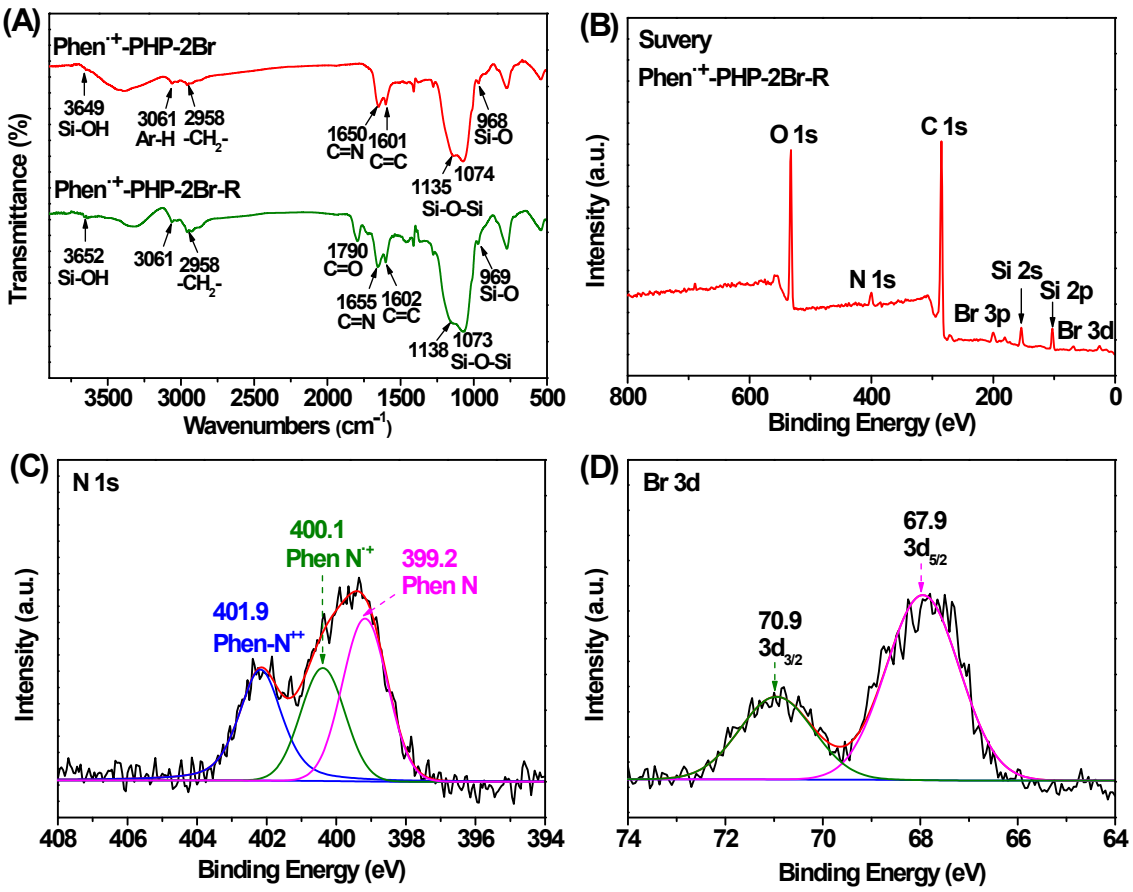

Fig. S26 Characterizations of the reused catalyst Phen$^{\bullet+}$-PHP-2Br-R: (A) FTIR, (B) XPS survey, (C) XPS N 1s, and (D) XPS Br 3d.

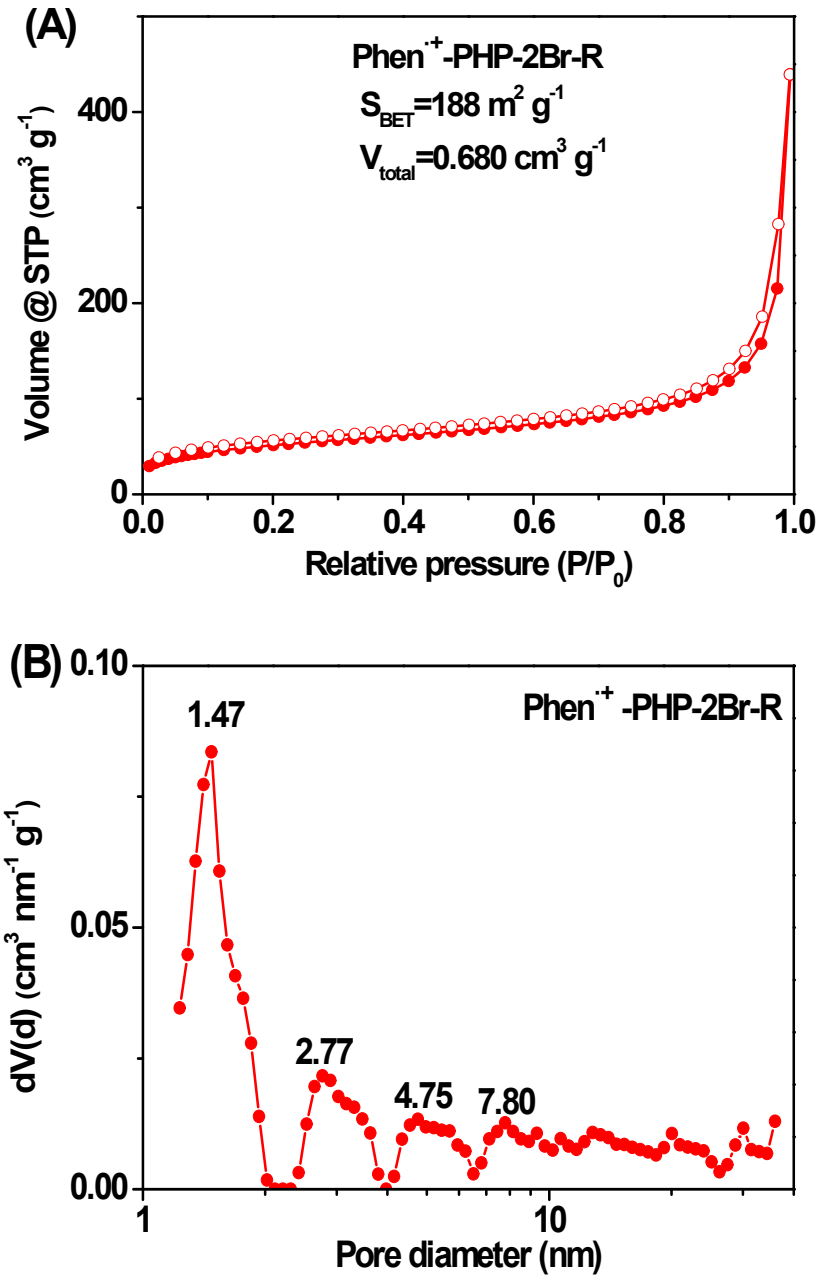

Fig. S27 (A) N_2 adsorption-desorption isotherm and (B) NLDFT pore size distribution of the reused catalyst Phen$^{\bullet+}$-PHP-2Br-R.

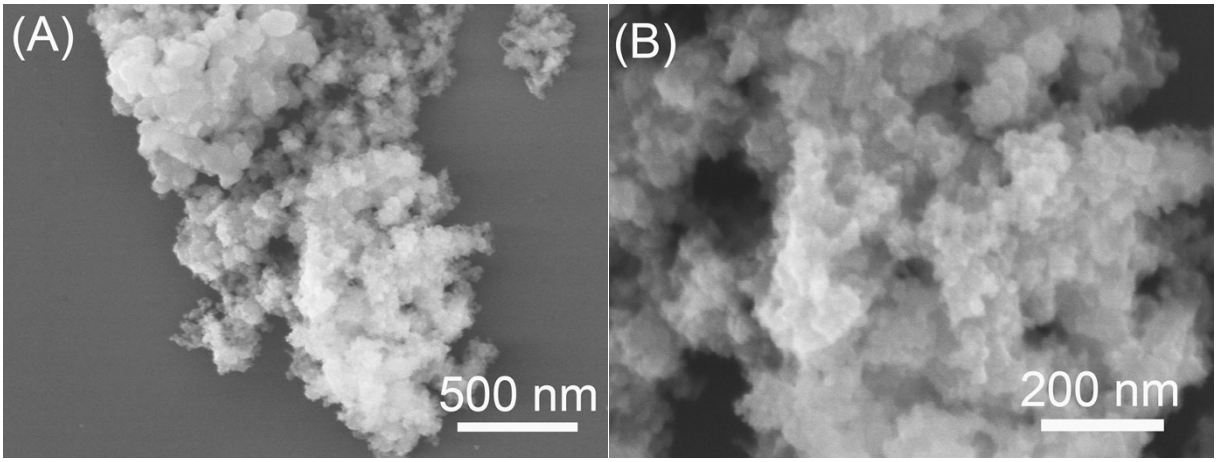

Fig. S28 (A, B) SEM images of the reused catalyst Phen$^{\bullet+}$-PHP-2Br-R.

Characterizations for the reused catalyst Phen$^{\bullet+}$-PHP-2Br-R.

FTIR and XPS characterizations were used to confirm the chemical structure and elemental composition of the reused catalyst Phen$^{\bullet+}$-PHP-2Br-R, as shown in Fig. S26. Compared with the fresh catalyst Phen$^{\bullet+}$-PHP-2Br, the FTIR and XPS spectra for N and Br elements in the reused catalyst Phen$^{\bullet+}$-PHP-2Br-R have no obvious changes, indicating its well-preserved chemical structure and composition. Besides, the reused catalyst was characterized by N_2 adsorption-desorption experiment (Fig. S27) and SEM images (Fig. S28). The S_{BET} (188 m^2 g^{-1}) and V_{total} (0.680 cm^3 g^{-1}) values of Phen$^{\bullet+}$-PHP-2Br-R only slightly decrease compared with the fresh catalyst, while the porous structure and morphology of Phen$^{\bullet+}$-PHP-2Br-R is also well retained by observing the SEM images.

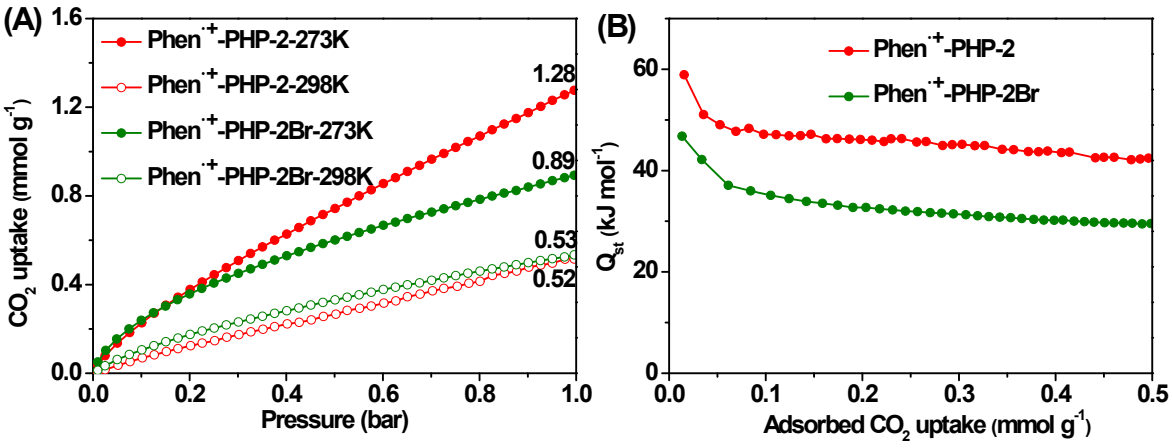

Fig. S29 (A) CO_2 adsorption isotherms of Phen$^{\bullet+}$-PHP-2 and Phen$^{\bullet+}$-PHP-2Br collected up to 1.0 bar at 273 K and 298 K. (B) The isosteric heat (Q_{st}) plots of CO_2 adsorption for Phen$^{\bullet+}$-PHP-2 and Phen$^{\bullet+}$-PHP-2Br calculated using the Clausius-Clapeyron equation.

References

S1 P. Zhao, M. Zhang, Y. Wu and J. Wang, *Ind. Eng. Chem. Res*., 2012, **51**, 6641-6647.

S2 Q. Zhou, M. Ye, W. Ma, D. Li, B. Ding, M. Chen, Y. Yao, X. Gong and Z. Hou, *Chem. Eur. J*., 2019, **25**, 4206-4217.

S3 E. Rafiee, S. Shahebrahimi, *J. Mol. Struct*., 2017, **1139**, 255-263

S4 S. Rezaei, A. Ghorbani-Choghamarani, R. Badri, A. Nikseresht, *Appl. Organometal Chem*., 2018, **32**, e3948.

S5 S. H. Hosseini, M. Tavakolizadeh, N. Zohreh, R. Soleyman, *Appl. Organometal Chem.*, 2018, **32**, 3953-3963

S6 K. Ahmed, G. Saikia, S. Paul, S. D. Baruah, H. Talukdar, M. Sharma and N. S. Islam, *Tetrahedron*, 2019, **75**, 130605.

S7 Q.-L. Tong, Z.-F. Fan, J.-W. Yang, Q. Li, Y.-X. Chen, M.-S. Cheng and Y. Liu, *Catalysts*, 2019, **9**, 791.

S8 O. Buyukcakir, S. H. Je, D. S. Choi, S. N. Talapaneni, Y. Seo, Y. Jung, K. Polychronopoulouc and A. Coskun, *Chem. Commun*., 2016, **52**, 934-937.

S9 H. Zhong, Y. Su, X. Chen, X. Li, R. Wang, *ChemSusChem*, 2017, **10**, 4855-4863.

S10 J. Wang, W. Sng, G. Yi and Y. Zhang, *Chem. Commun*., 2015, **51**, 12076-12079.

S11 O. Buyukcakir, S. H. Je, S. N. Talapaneni, D. Kim and A. Coskun, *ACS Appl. Mater. Interfaces*, 2017, **9**, 7209-7216.

S12 T.-T. Liu, R. Xu, J.-D. Yi, J. Liang, X.-S. Wang, P.-C. Shi, Y.-B. Huang and R. Cao, *ChemCatChem*, 2018, **10**, 2036-2040.

S13 X. Wang, Y. Zhou, Z. Guo, G. Chen, J. Li, Y. Shi, Y. Liu and J. Wang, *Chem. Sci*., 2015, **6**, 6916-6924.

S14 Q. Sun,Y. Jin, B. Aguila, X. Meng, S. Ma and F.-S. Xiao, *ChemSusChem*, 2017, **10**, 1160-1165.

S15 S. Subramanian, J. Oppenheim, D. Kim, T. S. Nguyen,W. M.H. Silo, B. Kim, W. A. Goddard III and C. T. Yavuz, *Chem*, 2019, **5**, 3232-3242.

S16 Y. Xie, Q. Sun, Y. Fu, L. Song, J. Liang, X. Xu, H. Wang, J. Li, S. Tu, X. Lu and J. Li, *J. Mater. Chem. A*, 2017, **5**, 25594-25600.

S17 J. Li, D. Jia, Z. Guo, Y. Liu, Y. Lyu, Y. Zhou and J. Wang, *Green Chem.*, 2017, **19**, 2675-2686.

S18 Y. Zhang, K. Zhang, L. Wu, K. Liu, R. Huang, Z. Long, M. Tong and G. Chen, *RSC Adv*., 2020, **10**, 3606-3614.

S19 Y. Chen, R. Luo, J. Bao, Q. Xu, J. Jiang, X. Zhou and H. Ji, *J. Mater. Chem. A*, 2018, **6**, 9172-9182.

S20 Y. Lei, Y. Wan, W. Zhong, D. Liu and Z. Yang, *Polymers*, 2020, **12**, 596.

S21 Z. Guo, Q. Jiang, Y. Shi, J. Li, X. Yang, W. Hou, Y. Zhou and J. Wang, *ACS Catal.*, 2017, **7**, 6770-6780.

S22 G. Chen, X. Huang, Y. Zhang, M. Sun, J. Shen, R. Huang, M. Tong, Z. Long and X. Wang, *Chem. Commun*., 2018, **54**, 12174-12177.

S23 Y. Zhang, K. Liu, L. Wu, H. Zhong, N. Luo, Y. Zhu, M. Tong, Z. Long and G. Chen, *ACS Sustainable Chem. Eng*., 2019, **7**, 16907-16916.

S24 G. Chen, Y. Zhang, J. Xu, X. Liu, K. Liu, M. Tong and Z. Long, *Chem. Eng. J.*, 2020, **381**, 122765.

S25 K. Hu, Y. Tang, J. Cui, Q. Gong, C. Hu, S. Wang, K. Dong, X. Meng, Q. Sun and F.-S. Xiao, *Chem. Commun*., 2019, **55**, 9180-9183.

S26 D. Ma, K. Liu, J. Li and Z. Shi, *ACS Sustainable Chem. Eng*., 2018, **6**, 15050-15055.

S27 Y. Zhang, G. Chen, L. Wu, K. Liu, H. Zhong, Z. Long, M. Tong, Z. Yang and S. Dai, *Chem. Commun*., 2020, **56**, 3309-3312.